Marine and Petroleum Geology
July 2019, Volume 105 Pages 293-312
https://doi.org/10.1016/j.marpetgeo.2018.07.017
https://archimer.ifremer.fr/doc/00752/86414/

The Zambezi delta (Mozambique channel, East Africa): High resolution dating combining bio- orbital and seismic stratigraphies to determine climate (palaeoprecipitation) and tectonic controls on a passive margin

Ponte Jean Pierre [1], Robin Cécile [1, *], Guillocheau François [1], Popescu Speranta [2], Suc Jean-Pierre [3], Dall'asta Massimo [4], Melinte-Dobrinescu Mihaela C. [5], Bubik Miroslav [6], Dupont Gérard [4], Gaillot Jéremie [4]

[1] Univ Rennes, CNRS, Géosciences Rennes – UMR 6118, 35000, Rennes, France
[2] Geobiostratdata Consulting, 385 route du Mas Rillier, 69140, Rilieux-la-Pape, France
[3] Sorbonne Universités, UPMC University Paris 06, CNRS, Institut des Sciences de la Terre de Paris (iSTeP), UMR 7193, 4 Place Jussieu, 75005, Paris, France
[4] TOTAL, Research and Development, Avenue Larribau, 64018, Pau Cedex, France
[5] National Institute of Marine Geology and Geoecology (GeoEcoMar), 23-25 Dimitrie Ociul Street, RO-024053, Bucharest, Romania
[6] Czech Geological Survey, Leitnerova 22, 60200, Brno, Czech Republic

* Corresponding author : Cécile Robin, email address : cecile.robin@univ-rennes1.fr

Abstract :

The Zambezi Delta draining the Southern African Plateau and the southern part of the East African Rift is one of a the largest delta of Africa with a long-lasting history starting during Early Cretaceous with more than 12 km of sediments deposited. The Zambezi Delta is therefore a unique archive of the past topographic evolution of southern and eastern Africa and their related deformations, but also of the climate changes, global and regional (consequences of local topographic growths). Understanding this archive supposes to get a high-resolution dating of the sediments. Our two objectives are here (1) to construct an age model of the Zambezi Cenozoic delta using a combination of biostratigraphy, orbital stratigraphy and sequence stratigraphy and (2) to determine the palaeoprecipitation variations of the Zambezi catchment from the Oligocene to present day in a known tectonic framework. The Neogene sequences were dated at high-resolution assuming that the third order sequences are of eustatic origin and record long-term eccentricity cycles. The sequences were correlated in ages on the calculated Earth orbital solutions of Laskar for the time intervals provided by the biostratigraphy (nannofossils, planktonic foraminifers). The palaeoprecipitation record was based on the definition of a humidity index based on pollen analysis and associated botanical associations. The late Oligocene was a quite wet period getting dryer in the uppermost Chattian. The base Tortonian (11 Ma) was a humid period. The Messinian was a dry period with a slight increase of the humidity during the Zanclean and a sharp increase around the Zanclean-Piacenzian boundary. The Zambezi Delta has recorded the uplifts of the Southern African Plateau (around 85 Ma and around 25 Ma) and those of the southward migration of the East African Rift (since 5.5 Ma).

Graphical abstract

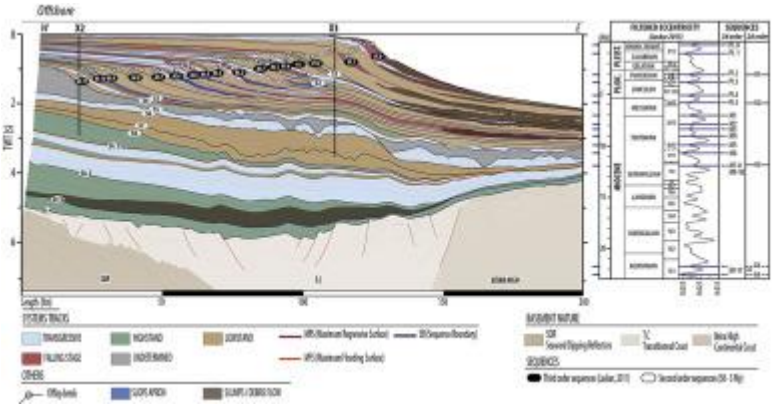

Highlights

► Dating sediments with a resolution of 0.1 Myr combining seismic stratigraphy, biostratigraphy an orbital stratigraphy. ► Quantifying palaeoprecipitations using a humidity index on botanical associations from pollens. ► Characterization of uplifts at 85 and 25 Ma (South African Plateau) and 5.5 Ma (migration of the East African Rift).

Keywords : Mozambique, Zambezi, Seismic stratigraphy, Orbital stratigraphy, Palaeoclimate

1. Introduction

The Zambezi Delta (Fig. 1) currently drains the South African Plateau (NE portion of the Kalahari Basin; (Thomas and Shaw,1988; Moore and Larkin, 2001) and the southern portion of the East African Rift (Fig. 1) and has the third largest catchment (1 320 000 km^2) in Africa, after the Nile and the Congo. Its current sediment load is not well known, but is estimated to range from 20.10^6 to 48.10^6 t/yr (Milliman and Syvitski, 1992).

Across all geological eras, the Zambezi Delta is the longest operating delta in Africa starting in the Early Cretaceous with more than 12 km of sediments deposited with 5 km during the Cenozoic (Salman and Abdula, 1995) and with no gravitary tectonics due to the absence of a major decollement level.

The size and location of the Zambezi River catchment has changed throughout the geological eras, and in the most recent times it also captures the upstream portion of the Limpopo River (Nugent, 1990; Moore et al., 2007). These changes resulted from deformation of the South African Plateau when it was uplifted during the Late Cretaceous and Oligocene (De Wit, 2007; Braun et al., 2014) and deformation of the East African Rift System (EARS) (Chorowicz, 2005) with formation of the Malawi Rift, which is assumed to have occurred in the late Miocene (Ebinger, 1989; Ebinger et al., 1993).

The topographic growth of EARS domes and rift shoulders had a first order impact on climate change in East Africa (Sepulchre et al., 2006), influencing atmospheric circulation, moisture transport and spatial patterns of precipitation, and therefore sedimentary flux of the deltaic systems (Milliman and Syvitski, 1992). Several studies have focused on changes in palaeoclimate that occurred in the EARS (e.g. Jacobs and Herendeen, 2004; Trauth et al., 2005;

Sepulchre et al., 2006; Vincens et al., 2006; Bonnefille, 2010; Feakins et al., 2013; Rasmussen et al., 2017), but only the study of Bonnefille (2010) summarised the continuous climate record since the late Miocene.

The Zambezi Delta is a unique archive (its long duration and absence of gravitary tectonics preserve the geometry of depositional sequences) for studying the influences of deformation and climate controls on the delta and its upstream catchment. Doing so requires high-resolution (around 1 Ma) age calibration of deltaic infilling.

Our study had two objectives: (1) construct an age model of the Zambezi Cenozoic delta using a combination of biostratigraphy, orbital stratigraphy and sequence stratigraphy, and (2) determine the precipitation record of the upstream catchment of the Zambezi Delta from the Oligocene to present day. We developed a new method using high-resolution cycles defined on seismic lines (seismic stratigraphy) to design an age model that combines biostratigraphy and orbital stratigraphy (which is the new feature).

The study is based on subsurface data: (1) seismic reflection lines for seismic stratigraphic analysis and (2) wells with well logs for seismic calibrations using lithology, age and drill cuttings to explore the micropaleontology (calcareous nannofossils, planktonic foraminifera) and palynology (pollen grains and spores).

2. Methodology

2.1. Data

The study is based on a set of 2D seismic reflection data shot in 1970s and 1980s and four petroleum wells (X, X1 to X3, Fig.1) drilled in the 1970s located on seismic profiles with well-logs and cuttings, provided by TOTAL.

2.2. Seismic stratigraphy

Since the 1970s, several successive approaches to seismic stratigraphy have been developed which are more complementary than in opposition.

Researchers at Exxon developed the first approach (Brown and Fisher, 1977; Mitchum et al., 1977), which is based on subdividing depositional sequences into system tracts to identify relative sea level variations in the sedimentary record and now known as the balance between the accommodation space (Jervey, 1998) and the sediment flux (see Neal and Abreu, 2009 and Abreu et al., 2011 for a review). System tracts, corresponding to stages of the relative sea level variations (Fig. 2), are bounded by three stratigraphic surfaces with truncations: (1) the unconformity (Un or sequence boundary SB) below onlaps, (2) the Maximum Flooding Surface (MFS) below downlaps, and (3) the Maximum Regressive Surface (MRS, formerly Transgressive Surface or Flooding Surface) above toplaps (Fig. 2). Some criticism was launched against this revolutionary model in the early 1980s. For example, no shoreline deposits were preserved when the relative sea level fell. Plint (1988) and Hunt and Tucker (1992) suggested defining a new system tract, the Forced Regressive Wedge System Tract (FRWST), which corresponds to sediments deposited during the fall in relative sea level.

Researchers at Norsk Hydro (Helland-Hansen and Gjelberg, 1994; Helland-Hansen and Martinsen, 1996; Helland-Hansen and Hampson, 2009) developed a technique based on the offlap break (shoreline or shelf-edge break) trajectory over time by defining stratal patterns: forced (descending) regressive, normal (ascending) regressive and transgressive (see Fig. 2 for its relations with relative sea level variations and Exxon's approach). In 2009, Catuneanu and 28 co-authors synthetized and standardised the approaches used to define the relation between the system tract, stratigraphic surfaces and clinoform geometry.

A depositional sequence is here defined as follows:

- the sequence boundary that corresponds to the first correlative conformity (CC, Catuneanu et al., 2009) and the onset in continental domain to the subaerial unconformity, an erosion surface overlain by onlapping strata;
- the forced regressive (FR) deposits (Catuneanu et al., 2009) (equivalent of the forced regressive wedge system tract of Hunt and Tucker (1992) or the falling-stage system tract - FSST - of Plint and Nummedal, 2000), which are not in the Exxon's model, correspond to descending regressive shorelines (i.e forced progradation) passing toward the deep-sea plain to the basin floor fan;
- the lowstand normal regressive (LNR) deposits (Catuneanu et al., 2009) which correspond to the lowstand system tract (LST) of Posamentier and Vail (1988) or ascending regressive shorelines (i.e progradation-aggradation) of Helland-Hansen (e.g. Helland-Hansen and Hampson, 2009);
- the maximum regressive surface (MRS), which corresponds to the former transgressive or flooding surface (Posamentier and Vail (1988) above the toplapping strata;
- the transgressive deposits (T; Catuneanu et al., 2009) which correspond to the transgressive system tract (TST) of Posamentier and Vail (1988) or transgressive shorelines (i.e retrogradation) of Helland-Hansen (e.g. Helland-Hansen and Hampson, 2009);
- the maximum flooding surface (MFS) which lies below downlapping strata;
- the highstand normal regressive (HNR) deposits (Catuneanu et al., 2009) which correspond to the highstand system tract (HST) of Posamentier and Vail (1988) or ascending regressive

shorelines (i.e progradation-aggradation) of Helland-Hansen (e.g. Helland-Hansen and Hampson,2009).

Based on their cause - climate or lithosphere deformation, relative sea level variations occurred over different durations in past geological periods (Graciansky et al., 1998). As a consequence, the stratigraphic record is a stacking of different orders of nested sequences. Determining the hierarchy of depositional sequences (between two sequence boundaries) or stratigraphic cycles (between two MFS) on a 2D section is difficult due to changes in the sedimentation rate over time. Vail et al. (1977) and Vail et al. (1991) defined orders of sequences based on their duration (first order: around 100 - 200 Myrs, second order: several 10 Myrs, third order: several 1 Myrs, fourth order: several 100 kys). This indicates that dating is required to determine a suitable hierarchy of sequences and cycles.

2.3. Sediment dating: age model

As mentioned in the introduction, the high-resolution dating (expected around several 0.1 Ma) of the Neogene sediments is based on a combination of biostratigraphy, orbital stratigraphy and sequence stratigraphy. The temporal resolution of planktonic foraminifer and calcareous nannofossil biozones (Gradstein et al., 2012) ranges from several 100 kys to several Myrs for the Neogene, which is not high enough for our study.

Increasing the temporal resolution is here based on two approaches (see discussions below). The first is biostratigraphic, examining strata boundaries using cuttings to provide a possible age range for formations. The second is orbital stratigraphic, based on identifying depositional sequences that may have been influenced by climate-induced sea level variations related to variations in the Earth orbit.

2.4. Biostratigraphy

The studied samples are ditch raw cuttings collecting sediments of a few centimetres in thickness. The samples were analysed for both foraminifers (with a special focus on the planktonic species) and calcareous nannoplankton analyses. Foraminifera were extracted from disintegrated sediment in a warm solution of sodium carbonate (Na_2CO_3); residue was sieved at 50 µm, 150 µm and 250 µm. Calcareous nannofossils have been studied in the fraction of 2-30 µm, separated by decantation method. Smear-slides have been analysed at an Olympus transmitting light microscope, with 1200x magnification. The occurrence of each species has been considered (Tables 1-4 in Supplementary materials) with respect to their distribution range in the biostratigraphic zonations (Martini, 1971; Bolli and Saunders, 1985; Perch Nielsen, 1985a,b; Berggren et al., 1995; Burnet, 1998; Young, 1998; Olsson et al., 1999; Berggren and Pearson, 2005; Pearson et al., 2006; Raffi et al., 2006; Gradstein et al., 2012). In addition, we particularly paid attention to some biostratigraphic markers displayed on Figures 8 and 9, which benefit from a robust age of appearance/disappearance datums obtained by astronomical tuning of several cored long sections (Raffi et al., 2006; Gradstein et al., 2012; Zeeden et al., 2013). The studied samples are rich in specimens of planktonic groups of organisms. The main limit of this approach is the use of cuttings and not in situ data such as clabs or cores, unfortunately not enough available in the case of this study. Cuttings are subject to cavings at time of drilling. This means that for a given level microfossils of younger sediments can be mixed with in situ specimens. This implies that the age of the level that has to be dated must correspond to the oldest microfossils available. To strengthen the chronological model, we used the data of all the four studied and/or considered wells, some of them being subject to more cavings due to the quality of drilling or the type of microfossils. In some samples, the mixing of (caved, reworked,

in situ) individuals of species of various ages is so high that we constrained the age with respect to equence stratigraphy (prism of low sea level or of high sea level) and then checked out which microfossils are consistent with it.

Analyses of calcareous nannoplankton were performed on all the studied samples (wells X1 and X3) with almost continuously consistent results. They were completed by analysis of planktonic foraminifera in some relatively uncertain intervals from the biostratigraphical viewpoint. The dated surfaces were first identified along seismic lines, as they must belong to the same reflector. In a second step, they are located on well-logs used for log drawings according depth velocity laws built for each wells. The surface age was defined using the oldest consistent microfossils identified along the surface of the two wells biostratigraphically studied (X1 and X3) plus some available unpublished biostratigraphic data already acquired on two other wells and provided by Total.

2.5. Orbital stratigraphy combined with seismic stratigraphy

The seismic stratigraphy study of the progradational Neogene sediments of the Zambezi delta shows the existence of stratigraphic depositional sequences organized in similar repetitive stratigraphic motif with a duration around 1 Myr (third order cycles). This is a characteristic feature of most of the world deltaic systems at that period (e.g. Baltimore Canyon Margin: Greenlee and Moore, 1988, Carnavon Basin: Cathro et al., 2003..). Based on these observations, P.R. Vail and his group (Bartek et al., 1991) defined for the Neogene a world-scale pattern of third order sequences of eustatic origin due to ice volume variations at the base of the Exxon's chart (see Hardenbol et al., in Graciansky et al., 1998).

Since the 1990s and this idea of global eustatic third-order sequences for Mio-Pliocene times, three major advancements have been made. (1) Third order cycles are recognized as resulting from sea level variations of climatic origin related to the Earth orbital parameters variations (e.g. Strasser et al., 2000; Boulila et al., 2011; Martinez and Dera, 2015..). (2) These cycles are due to long-term eccentricity variations with frequencies of several million years, around 1.2, 2.4 and 9 Ma. Laskar (Laskar et al., 2004, 2011) calculated long-term orbital solutions at eccentricity time-resolution for Cenozoic times. (3) This pattern is different from the Pleistocene one characterized by climatically-enhanced orbital frequencies (40 kyr: Early Pleistocene, 100 kyr: Middle-Late Pleistocene).

The periods of low eccentricity correspond to cold climates, while high eccentricity periods correspond to warm climates. For pre-Pleistocene times and at the time-scale of few million years (see Hansen et al., 2013), the cold climate periods are coeval to ice volume decrease (e.g. de Boer et al., 2010) and then to sea level lowering (e.g. Miller et al., 2011) and the contrary for the warm climate intervals.

Correlation between an eustatic curve and the stratigraphic record supposed to know the sedimentary flux (Jervey, 1988). Both the MFS (maximum flooding surface) and the MRS (maximum regressive surface) occurred at time of balance between relative sea level rise and sediment supply/production. They cannot be used for correlation to a curve proxy of the sea level variations, as expected here. The only stratigraphic surfaces in marine environments controlled by the relative sea level variations and therefore independent of the sediment supply/production, are the correlative conformities (Fig. 2). These surfaces are formed during the relative sea level high and low periods. The time interval between the two correlative conformities corresponds, onshore to the erosion of the subaerial unconformity (SU) and, offshore to the formation of the

forced regressive (FR) deposits. We here used as a time-line the first correlative conformity or sequence boundary, period of high relative sea level and onset of the unconformity

The procedure of dating is a follow.

- Biostratigraphic dating of a single, or sets of, repetitive third-order depositional sequence(s) provide age ranges with a resolution of several million years.
- Use of Laskar's orbital solutions (Laskar et al., 2011) and, within the time range obtained from biostratigraphy, third order sequence boundaries (first correlative conformity) are correlated with the maxima of the Earth eccentricity.
- The date of the sequence boundary is the one of the maximum of Earth eccentricity calculated by Laskar.

2.6. Pollen and spore analysis and inferred palaeoprecipitation variations

At least one hundred pollen grains were counted per sample except in one very poor sample (Tables 5-6, Supplementary materials). Pollen grains were obtained after acid treatments using HCl, HF, and HCl again, followed by concentration in $ZnCl_2$ (at density 2.0) and sieving at 10 µm; a 50 µl volume of residue was mounted in glycerol and examined under a light microscope (magnification: x1000). One hundred and thirteen taxa[1] were identified in the ten samples from well X1, one hundred and twenty-eight taxa were identified in the twenty eight samples from well X1. They were gathered into eleven groups relative to the main types of the modern vegetation of Africa, represented today along the Zambezi catchment. Botanical identification of pollen grains is for long used in Quaternary and Neogene records thanks to a detailed morphological examination of fossil pollen and comparison with pollen databases of

[1] A taxon (pl. taxa) is an entity in Systematics that may be a family, a genus or a species

living plants (slide and photograph collections, atlases, special papers) originating from herbarium specimens (Suc et al., 2004). It has been established that the same approach is also suitable for Paleogene deposits (Suan et al., 2017).

Pollen flora of well X1 concerns in a discontinuous record the late Oligocene and late Miocene clayey sediments of continental origin (Figs. 6-7). Studies on modern sediments from the Grand Rhône Delta (SE France) show that pollen grains recorded in such deltaic to protodeltaic sediments are almost exclusively transported by the river (Cambon et al., 1997) and are highly representative of the vegetation of the catchment basin (Beaudouin et al., 2005a). Studies on recent Quaternary similar sediments from the Gulf of Lions (offshore SE France) evidenced weak reworking of palynomorphs (i.e. pollen grains and spores) during phases of high sea level, increasing during phases of sea-level fall (Beaudouin et al., 2005b). Pollen flora of well X3 comes from late Miocene to middle Pleistocene hemipelagic shales and silts (Figs. 6-7). Researches done on modern deeper deposits in an area influenced by a powerful river such in the Gulf of Lions may guide our interpretation of pollen record of well X3: sediments from the shelf and slope are rich in pollen grains without sorting by marine currents that makes the signal understandable and reliable where reworking is detected with respect to preservation and colour (Beaudouin et al., 2007a,b); pollen signal from recent turbidites of the Rhône Neofan (Gulf of Lions) appeared not much disturbed by comparison with a shelf pollen record, despite more intense reworking in relation with phases of low sea level (Beaudouin et al., 2004). In addition to ancient morphological types obviously reworked, palynomorphs of wells X1 and X3 have been considered as reworked when they were poorly preserved or affected by a dark colouring (Tables 5-6, Supplementary materials Pollen grains affected by caving cannot be detected because of the

almost constant representation of the different vegetation types. Nevertheless, consistency of the slight fluctuations observed in pollen assemblages leads to consider cavings as negligible.

The modern catchment of the Zambezi River displays a large variety in vegetation resulting from strong climate contrasts between the west, arid - the Kalahari Desert - and the east, very humid around the Malawi Lake (Fig. 3). From the thermal viewpoint, some patches of tropical rain forest persist in spite of human activity in addition to the mangrove on the coastline, that contrasts with few relict areas with Afromontane forest the representation of which is impossible at the scale of the map (Fig. 3).

In Tables 5 - 6 (Supplementary materials displaying the detailed pollen records from wells 1 and 3 respectively, taxa have been grouped according to their ecological significance in eleven groups representative of the regional vegetation types (Fig. 3). These groups allow drawing the synthetic pollen diagrams shown in Fig. 11, their respective percentages are calculated on the total pollen sum (Tables 5-6, Suppl. mat.). Such diagrams contribute to define a dominant climate in the region according to the prevalent pollen-ecological groups.

In the case of rather constant relative frequencies of the pollen groups as shown in the synthetic pollen diagrams of wells 1 and 3 (Fig. 11), calculation of pollen ratios between climatically opposed taxa or groups of taxa may be used to spotlight some variations difficult to evidence (Cour and Duzer, 1978). Such ratios are seldom used in African palynology (Dalibard et al., 2014). In the pollen record of wells 1 and 3, it appeared worthwhile to consider the pollen ratio tropical rain forest + warm-temperate semi-deciduous forest + pioneer forest / sparse forest to wooded savannah + dry grassland to open savannah, i.e. low altitude forest vegetation (humid context) vs. open vegetation (dry context). Taking into account the important contrast in humidity between these assemblages, the ratio can be regarded as a Humidity Index (HI). Its values ≤ 1

mean drier climatic conditions while those ≥1 mean more humid ones. This HI cannot be directly calibrated in terms of annual rainfall because we have no surface pollen records from different climatic areas of the catchment basin. However, DeBusk (1997) realised pollen analysis of surface samples of Lake Malawi located at about 500 m in altitude. A rough calculation on this record of the pollen ratio between evergreen forest / grassland shows a strong contrast between the northernmost part of the lake covered by forests and its southernmost part inhabited by wooded savannah (Timberlake, 2000). To the north where precipitation is of ca. 2400 mm/yr, the ratio would range from 0.133 to 0.555. To the south where precipitation is lower than 800 mm/yr, the ratio would range from 0.042 to 0.077.

3. Geological setting

The Zambezi Delta is located along the northern Mozambican Margin, which is bounded by two major transform fracture zones (F.Z.) (Fig. 1A), the Mozambique F.Z. to the west and the Davie Ridge or Davie F.Z. to the east. The Zambezi Delta is bounded in the south by the Beira High and passes laterally into a deep-sea plain, the Angoche Basin (Fig. 1A).

3.1. Geodynamic setting

The Mozambique Margin is the result of the Mozambique oceanic domain opening between Africa and Antarctica during the Gondwana break-up. The age of the first oceanic crust is still debated, with a range from 155.3 Ma (M26) (Jokat et al., 2003; Konig and Jokat, 2010) to 166 Ma (M41) (Leinweber et al., 2013; Leinweber and Jokat, 2012), i.e. the Late Jurassic. The Beira High is a 280 km long and 100 km wide continental topographic structure that runs parallel to the coast (Konig and Jokat, 2010; Mueller et al., 2016), dividing the Zambezi sedimentary

system into a proximal part including the deltaic domain and the Zambezi depression, and a distal part corresponding to turbidite deposits.

Onshore, the Zambezi catchment drains a large area from the northern boundary of the South African Plateau (Thomas and Shaw, 1988) to the southern portion of the EARS, including the eroded aborted Karoo Rifts (Luangwa, Cabora Bassa, Mid-Zambezi) and active Neogene Rifts (Malawi/Shire). The Zambezi River path is subdivided into three major segments with specific geomorphic characteristics (Moore et al., 2007). Upper Zambezi, which extends from the headwaters to Victoria Falls; Middle Zambezi, which extends from the Falls to the edge of the Mozambique coastal plain, corresponding to the Cabora Bassa Gorge; and, Lower Zambezi, which is located along the coastal plain (Fig.1B).

This segmentation results from topographic changes in the Zambezi in response to three main deformation events that have occurred since the Cretaceous (Moore et al., 2007) caused by uplifts of the South African Plateau and the EARS (Fig. 4).

- The initial uplift of the South African Plateau in the Late Cretaceous, which most likely induced a flexure from the Limpopo to Zambezi Rivers, as identified by Du Toit (1933) and later described by Moore (1999) as the Okavango-Kalahari-Zimbabwe high. Apatite fission track analysis (AFTA) recorded this event in southern Africa (e.g. (Gallagher and Brown, 1999; Van Der Beek et al., 2002)), showing a main denudation event and an increase in the amount of sediment (Guillocheau et al., 2012).

- A second uplift of the South African Plateau from the Oligocene to the beginning of the Miocene. This long-wavelength deformation induced a progressive tilt of the Zambezi Margin and relief denudation, as indicated by AFTA (Belton and Raab, 2010; Emmel et al.,

2014) and tilted sedimentary deposits (Cheringoma Fm and Urrongas Fm in southern Mozambique) (Flores, 1973).

- The third event corresponds to the progressive southward migration of the EARS since the Oligocene (Chorowicz, 2005; Macgregor, 2015) coeval with an increase in topography roughness and relief (Pik et al., 2008). The EARS is subdivided into a western branch, which crosses Mozambique and delimits the Rovuma and Victoria plates from the African plate, and an eastern branch, which crosses Tanzania and spreads into the Mozambique Channel through the Davie Ridge (Mougenot et al., 1986). It delimits the Rovuma from the Somalian plates.

Uplift of the EARS began in its eastern branch (in Ethiopia) during the Oligocene-Miocene, with long-wavelength topographic growth contemporaneous with Oligocene volcanic activity (LIP, Couli et al. (2003) overlapping the Ethiopian Rift shoulders (Pik et al., 2003, 2008). The initial western branch of the EARS developed during the middle Miocene (Macgregor, 2015) with the formation of Lake Albert at about 17 Ma (Simon et al., 2017), the central Tanganyika Rift at approximately 9-12 Ma (Cohen et al., 1993), and the Malawi Rift most likely at 8.6 Ma (Songwe tuff) (Ebinger, 1989; Ebinger et al., 1993). More recently, thermochronological data recorded a regional uplift dated at 2.5 Ma (MacPhee, 2006; Bauer et al., 2016) and K/Ar volcanic activity dating (Ebinger et al., 1993) from the Albert Rift to the North Malawi Rift. This major tectonic activity since the Oligocene has shaped a 6000 km elevated area (Chorowicz, 2005) that is oriented mainly north-south with a medium wavelength crest that reaches 1500-5100 m.

3.2. Margin infilling

The Zambezi sedimentary record is assumed to have started during the Late Jurassic, deposited over Karoo volcanics in the Early Jurassic (Salman and Abdula, 1995) (Fig. 4). The

Late Jurassic sediments are continental sandy red-beds distributed mainly along buried grabens. Cretaceous rocks are terrigenous sediments deposited in continental and shallow marine environments (Sena, Domo (Lower and Upper), and Lower Grudja Fm). Cenozoic deposits are predominantly marine and deltaic (Salman and Abdula, 1995) (Fig. 4). The Paleogene is characterized by a shallow, mixed marine platform (Upper Grudja Fm), the Eocene by a carbonate platform (Cheringoma Fm). The base of Oligocene corresponds to the initiation of the two main present-day deltaic systems, the Limpopo and the Zambezi Deltas (Salman and Abdula, 1995).

3.3. Climate setting

Several methods have been used to study changes in the East African paleoclimate: computer modelling (Sepulchre et al., 2006); analysis of sedimentary rocks such as bauxites or evaporites (Scotese et al., 1999; Burke and Gunnell, 2008; Morley, 2011) and analysis of palaeobotanical data such as leaves (Jacobs and Winkler, 1992; Jacobs and Herendeen, 2004), fruit (Chesters, 1957), pollen grains (Vincens et al., 2006; Bonnefille, 2010; Rasmussen et al., 2017), and wood (Bonnefille, 2010). In addition, several studies analysed leaf morphology to quantify palaeoprecipitation (Jacobs, 2002; Jacobs and Herendeen, 2004). Most studies are based on scattered outcrops in northeast Africa; only Bonnefille (2010) provides a continuous curve of vegetation associations characteristic of climate zones, based on pollen record from well DSDP 231 (Gulf of Aden). These discontinuous data hinder understanding of climate change in an active tectonic setting in which local vegetation is the result of interactions between topography and climate (Jacobs et al., 2010). Thus only major climate trends can be identified:

Paleocene : The Paleocene was a wet and warm period characterised by a widespread megathermal rainforest or monsoon forest (Morley, 2011) and lateritic rocks from 23°N to 23°S latitude (Burke and Gunnell, 2008).

Eocene : The Eocene corresponds to the wettest and warmest period of the Cenozoic, with deep sea water temperatures 10°C higher than those of the present day (Zachos et al., 2001). As in the Palaeocene, a megathermal rainforest or monsoon forest covered most of Africa (Burke and Gunnell, 2008; Morley, 2011). However, palynological data indicate that woodlands existed in Tanzania during the Lutetian at 46 Ma (Herendeen and Jacobs, 2000; Jacobs and Herendeen, 2004), which challenges the idea of a permanent megathermal forest over Africa (Bonnefille, 2010).

Oligocene : The Oligocene defined at its outset by global climate change, with the growth of the Antarctic ice sheet and a 5°C decrease in deep-sea water temperatures (Zachos et al., 2001), which initiated an icehouse period. Locally, palynological data indicate the presence of moist forests in Ethiopia in the Chattian (Jacobs and Herendeen, 2004; Jacobs et al., 2005; Pan et al., 2006). However due to the lack of outcrops of this age over larger geographic areas, the extent and sustainability of this climate belt in East Africa is uncertain (Bonnefille, 2010).

Miocene : The Miocene is characterised by a climatic temperature optimum between 14.7 and 17.0 Ma (Langhian, Zachos et al., 2001) and rapid global cooling (Serravallian) caused by growth of a permanent Antarctic ice sheet (Zachos et al., 2001). East Africa experienced widespread aridification in the early to middle Miocene. The growth of relief and high volcanic activity related to the EARS is assumed to have created great variability and spatial heterogeneity in vegetation, with wet forests above drier plains and rain shadow effects that dried vegetation (Bonnefille, 2010). For the late Miocene, based on the continuous record of well DSDP 231 (Gulf

of Aden), Bonnefille (2010) highlights three pulses of grassland vegetation and one episode of reduction in pollen richness corresponding to the occurrence of wet events at 10.5, 7.0 and 5.5 Ma and an arid event at 6.5 Ma, respectively.

Pliocene : At world-scale the early Pliocene (5.3-3.6 Ma - Zanclean) is a warm period with two cooling (glaciation) events around 4.9-4.8 Ma and 4 Ma (De Schepper et al., 2014). The cooler upper Pliocene (Piacenzian) is punctuated by a warm period known as the Mid-Piacenzian (former mid-Pliocene) Warmth (or Warm Period) between 3.25 and 3.05 Ma (e.g. Prescott et al., 2014). The early Pliocene is an African-scale humid event (e.g. Bonnefille, 2010).

Pleistocene : The Pliocene - Pleistocene transition is a major cooling, followed at the early - middle Pleistocene transition (0.8-0.9 Ma) by a change in the climatic record of the prevailing influence of obliquity in the orbital cycles (41 kyrs) during the early Pleistocene replaced by that of eccentricity (100 kyrs) after. Historically, these variations were recorded in the peri-Sahara marine domains with the record of aeolian dusts in West and East Africa sediments (Tiedemann et al., 1994; deMenocal, 1995).

4. Results

4.1. Seismic stratigraphy (Fig.5-7)

Two types of depositional profiles were observed: a margin delta (most of the basin infilling) and a carbonate ramp. The profile of the margin delta changed over time, with an increase in height and steepness of clinoforms from the Cretaceous to the present day (from 80 to ~1400 m). The flat upstream portion (undaform or topset) consists of flat relatively continuous parallel to slightly divergent reflectors (Fig. 5). Calibration of the well logs and cuttings suggests that they are either continental deltaic plain deposits passing upstream to alluvial

plain deposits (sequences S6-S4) or, more recently, alternating deltaic plains and shelf deposits due to numerous marine floods (sequences S4-S1). The clinoforms have high amplitude reflectors that consist mainly of clayey siltstones. The base of the clinoforms (fondoform or bottomsets) shows a wide variety of facies, from gravitary deposits to hemipelagites. The gravitary deposits (Fig. 5) are either reflectors of differing degrees of continuity (alternating continuous and discontinuous sub-chaotic reflectors - shallow turbidite lobes) or are chaotic (Mass Transport Complexes (MTC): slumps to debris flows). The most obvious and common features are mounded structures with large aggradational sandwaves and channels characteristic of reworking and transport by oceanic currents (contourites s.l. ; e.g. Faugères et al., 1999; Rebesco et al., 2014 - Fig. 5) .

The carbonate ramp (sequences S7 and S6 - Figs. 6-7) is poorly documented on cuttings and outcrops (it crops out upstream in the Cheringoma Plateau; Fig. 1). It is made up of muddy limestones (calcilutites - mudlog descriptions) passing upstream to higher energy bioclastic facies (calcarenites - mudlog descriptions).

At least three orders of sequences (Figs. 6-7) were defined that require confirmation using the age model (see discussion above). The possible third order sequences, which are well recorded in the Oligocene-Neogene wedge (based on previously published ages see above), are repetitive stratigraphic motives. Seventeen sequences were defined and classified from the most recent (Pl.0, Pl.5) to the oldest (M1, M.11). Four main sub-units were defined, which correspond in part to system tracts:

- Gravitary deposits part of the of the FSST and/or LST onlap the unconformity at the toe of the clinoform. These deposits are either shallow turbidite lobes (see description above) along slope aprons or MTC.

- FR or FSST and LNR or LST deposits, were difficult to distinguish one from other. Most of these wedges are progradational-agradational indicating LNR or LST. Few periods of accommodation removal corresponding to FR or FSST are preserved. This is likely due to the large amount of subsidence created beneath the delta, which is often greater than the accommodation removal due to eustasy.
- Transgressive deposits (T or TST) which are retrogradational, highly aggradational wedges.
- A few well-preserved HNR deposits, whose dominant feature is the TST. Most are recorded by a single reflector below the unconformity or are eroded by the latter.

Potential second order unconformity-bounded sequences (Figs. 6-7) were defined above the main world-scale marine flooding of the Cenomanian-Turonian boundary (based on previously published ages see above). The sequences were classified from the most recent (S0) to the oldest (S8):

- Sequence S8 is mainly composed of siltstones. Offlap breaks were difficult to identify. The deposits present destabilization features and numerous erosion surfaces are observed.
- Sequence S7 is a mixed siliciclastic (mainly siltstones) carbonate (coarse grained bioclastic sands) ramp corresponding to the Upper Grudja Fm (Salman and Abdula, 1995), with offlap breaks that were difficult to identify. Oceanic current activity is substantial, as indicated by the numerous erosion surfaces along the distal ramp that increase toward the eastern portion of the Beira High.

- Sequence S6 is mainly a carbonate ramp with sediments that are finer grained than those in S7, with still active erosion and transport by ocean currents. It corresponds to the Cheringoma Fm (Salman and Abdula, 1995). A large contourite mound was created along the Beira High.

- Sequence S5 is bounded by the largest unconformity in the entire existence of the delta, with incisions along the shelf (flat-bottom incised valleys), the ramp/slope (canyons) and the deepest part of the system (contourite incised channels). Many older Eocene fauna are reworked in the sediments just above this unconformity. This is the birth of the modern delta, with a typical deltaic depositional profile. The clinoforms become higher, ranging from 650-900 m. Third order sequences are difficult to identify in this mainly progradational sequence consisting of coarse-grained sand upstream and silt downstream.

- Sequence S4 (third-order sequence: M.11) is bounded by the second largest truncated unconformity underlying progradational wedges and with a major onlap of the overlying sediments. This sequence is relatively thin (200 ms) and eroded along the Beira High by large contourite incisions.

- Sequence S3 (third-order sequences: M.10 to M.1) is bounded by an erosional unconformity truncating older inner deposits. The deltaic clinoforms progressively grow to more than 1000 m. This mainly progradational sequence is characterised by a FR wedge above the unconformity. This is the time of emplacement of the first shallow turbiditic wedges at the base of clinoforms. The first MTC occurred. The upstream sediments are coarse to medium-grained sands.

- Sequence S2 (third order sequences: Pl.5 to Pl.3), mainly progradational and aggradational, consists mainly of fine to medium grained sands and silts. The clinoforms range in height from ~1000 to ~1300 m, and MTCs are more common.

- Sequence S1 (third-order sequences: Pl.2 to Pl.0), mainly progradational and aggradational, is the growth period of the modern depositional profile (with clinoforms higher than 1400 m). MTCs are the dominant gravity deposits.

A first order cycle, or continental encroachment cycle (e.g. Graciansky et al., 1998), was defined. However Cenozoic uplifts eroded the upstream portion of the margin, which made it difficult to identify major marine floodings. Two plausible candidates are the MFS of the Cenomanian-Turonian boundary or sequence S6 (Cheringoma Fm). Geometrically, the trend is progradational to aggradational during the earliest Cretaceous from the basement to the sequence boundary Uc2 then clearly retrogradational until the MFS of the Cenomanian-Turonian boundary. It is more aggradational from the latter to the MFS of sequence S6, and it is progradational-aggradational from the MFS of sequence S6 to the seafloor forming the famous Oligocene-Neogene wedge characteristic of the Zambezi Delta.

4.2. Age model

Two types of age models were developed. For the Late Cretaceous and Paleogene, ages were based only on biostratigraphy (Figs. 6-7) (planktonic foraminifera and calcareous nannofossils - figs. 8-9). For the Neogene, a true age model was developed based on biostratigraphy (using the same proxies) and orbital stratigraphy combined with seismic stratigraphy (Fig. 10).

Late Cretaceous to Paleogene

- The sequence boundary of sequence **S8** was dated from planktonic foraminifera to the boundary between the *Dicarinella asymetrica* and *Globotruncanita elevata calcarata* biozones (well X2), and to that between *Globotruncanita elevata calcarata* and *Dicarinella concavata* on X1; i.e. around the Santonian-Campanian boundary.

- The sequence boundary of sequence **S7** (Upper Grudja Fm) is dated on the well X3 by both planktonic foraminifera and calcareous nannofossils between biozones UC16 (72-76 Ma, late Campanian) and NP4 (61.5-63.2 Ma, uppermost Danian) (calcareous nannofossils) and between *Gansserina Gansseri* (71.8-72.8 Ma, uppermost Campanian-base Maastrichtian) and P3a (61.2-62.2 Ma, uppermost Danian - base Selandian) zones (planktonic foraminifera). On the wells X2 and X1 it is only dated by planktonic foraminifera between *Abathomphalus Mayaroenis* (77.8-67.3 Ma, uppermost Campanian most of the Maastrichtian) and P3-P3a (62.2-60.7, Selandian) biozones (well X2), and between *Gansserina gansseri* and E5-P4c biozones (well X1). The uppermost Maastrichtian and the early Danian are missing, and no downward onlapping wedges that might be the early Danian missing in well X3 were identified from seismic lines. The early Danian seems a hiatus at the scale of the domain studied.

- The sequence boundary of sequence **S6** (Cheringoma Fm) is dated on wells X1 and X3 by both planktonic foraminifera and calcareous nannofossils between zones P5 and E3-E2 (X3), and E5-P4c and E7b (well X1) (planktonic foraminifera) and between zones NP9 and NP10 (well X3) and NP12-NP8 and NP15-NP14 (well X1) (calcareous nannofossils). In the well X2 the sequence boundary is only dated by planktonic foraminifera between P5-E2 and E4-E3 zones.

Integrating possible cavings the age of the oldest underlying formation belongs to the foraminifer zone P4c and the one of the oldest overlying formation refers to biozone E7b. According to the fact that the age of a formation might be at the early or latest time range of the biozone, minimum and maximum age ranges of the sequence boundary have to be defined. Here the minimum range is between 57.7 and 57.0 Ma and the maximum between 48.2 and 45.7., i.e. late Thanetian to early Lutetian. Considering the sequence S6 thickness evolution from wells X to X3, we suggest to set the age using a well with high sedimentation rate, i.e X3. A late Thanetian to early Ypresian age is most probable (57.7-54.5 Ma, i.e. NP9-NP10 biozones).

- Regarding to the planktonic foraminifera, the sequence boundary of sequence **S5** (base of the deltaic complex) is dated between zones E15-E14 and E14 (X3), intra zone E15-E9 (well X2) intra zone E14 (well X1); and between NP20-NP19 and NP18 zones (well X3), intra NP 17 zone (X1) for what concerns calcareous nannofossils. Based on the same principles than for S6, the age of the oldest underlying formation refers to zone E9 and the one oldest overlying formation belongs to zone E15 (maximum 43.2-43.8 Ma, minimum: 34.6-36.2 Ma). Because of the condensed toes of deltaic clinoformes observed on X2 and X3, we suggest to base the age on a well drilled in the deltaic clinoforms where the sedimentation rate is higher (X1). In that case, the ages of the oldest underlying formation and of the oldest overlying formation fall into the same biozones i.e. E14 (36.2-38.2 Ma, latest Bartonian to early Priabonian). It cannot be younger than the Eocene-Oligocene boundary (33.9 Ma) as previously expected by different authors (e.g. Salman and Abdullah, 1995).

- The sequence boundary of sequence **S4** is dated between zones O1-2 and M1-O7 (well X2) according to (planktonic foraminifera); and between NP25 and NN7 zones (well X1) and zones NP25 and NN4-5 (well X3) according to calcareous nannofossils.

  The age of the oldest underlying formation refers to zones O1-2 and the one oldest overlying formation to zone M1. The minimum age range of the sequence boundary S4 is between 30.2 and 34 Ma and the maximum between 25.2 and 21.7 Ma, i.e. from Rupelian to most of the Aquitanian. The hiatus in well X2 is quite long (i.e. Rupelian to Aquitanian). Therefore we suggest to use the well X1 where no hiatus is observed. Based on X1, the sequence boundary S4 is posterior to the O6 biozone (27-25.2 Ma), a late Chattian age (25-23 Ma) is most probable.

Neogene

Several age ranges were provided by calcareous nannofossils ticking either single or sets of third order cycles. These ages provide possible ranges for the equivalences with the Laskar's orbital solutions and therefore the age calibration of the third order sequence boundaries. The first satisfying result is that we got the same number of sequences on the Laskar's orbital solutions than the observed third order sequences using the ages provided by biostratigraphy. Base of sequence M7 (also base S3 sequence boundary) is dated at 11.9 Ma, and so on for base of M6 at 10.7 Ma, M5 at 9.9 Ma, M4 at 9.0 Ma, M3 at 8.4 Ma, M2 at 7.8 Ma, M1 at 7.0 Ma, Pl.5 (base S2 sequence boundary) at 5.8 Ma, Pl.4 at 5.0 Ma, Pl.3 at 3.8 Ma, Pl.2 (base S1 sequence boundary) at 3.0 Ma, Pl.1 at 1.0 Ma, Pl.0 at 0.2 Ma.

4.3. Palaeoprecipitation evolution (Fig. 11, Tables 5-6 Supplementary materials)

The synthetic pollen diagrams of wells X1 and X3 (Fig. 11) show that the distribution of each pollen group is quite uniform during the late Oligocene as from the late Miocene up to mid-Pleistocene. The late Paleogene to middle Pleistocene pollen flora of the Zambezi catchment is dominated by *Poaceae* representing open vegetation and *Cyperaceae* representing freshwater ecosystems, supporting a uniform permanent contrast between two environments, the dry tropical domain and the flat humid habitat (swamps to little lakes). Few littoral plants (halophytes, mangrove elements, components of the tropical rain forest and warm-temperate and pioneer forests) were recorded. This might be somewhat biased by the course of the Zambezi River that only crossed these domains at its end. On the whole, the pollen assemblages preserved in the sediments offshore of the Zambezi Delta denote almost continuous warm and dry climatic conditions.

However, few weak variations are perceived. An interesting point is the variations of the elements of the Afromontane forest, mainly composed of *Podocarpus* that indicates the occurrence of high relief in the region. Their slight increase in the early Chattian, mid-Tortonian, late Zanclean and especially Calabrian (Fig. 11) may result from descent of this vegetation belt in relation with some cooling (e.g. Dalibard et al., 2014), perhaps associated with a more intense activity of the river in altitude. Noteworthy is also the maximum of mangrove elements during Chattian and early Tortonian, probably in relation with warmer conditions and highstand of sea level (Poumot, 1989).

The most relevant proxy is the above defined Humidity Index (HI). Unfortunately the number of samples is quite limited for the late Oligocene and for the late Miocene. This is explained by the origin of the concerned samples within the condensed deposits of the toes of clinoforms. Obviously, late Oligocene (Chattian) is the most humid period of all the studied time

interval with values of HI comprised between 0.6 and 0.9 in well X1, that suggests yearly rainfalls of ca. 2000 mm. It occurred after a little aridification around the Eocene-Oligocene boundary compared to the very humid conditions prevailing up to Lutetian (Braun et al., 2014). Humidity was important again during Tortonian when HI values reached 0.75 in well X1. It is to be pointed out that the maxima of HI in the coastal well X1 are higher than those in the distal well X3, probably because of the lesser concentration in arboreal pollen grains towards the basin. After an aridification during the uppermost Miocene - lowermost Pliocene (?), humidity increased again during the late Pliocene with HI values reaching a maximum at 0.255 in well X3, but this phase was not so humid as the Chattian and Tortonian phases. Following repeated more arid conditions, the Gelasian-Calabrian period was more humid too with after all maximum HI values lower than 0.1. Apart from the more humid episodes, HI ranges between 0.2 and 0.3 in well X1 and 0.01 and 0.05 in well X3, revealing annual precipitation below 800 mm.

5. Discussion

5.1. Regional (lithosphere deformation) vs. global (eustasy/climate) controls of the second order sequences (Fig. 12)

The second order sequences are controlled as all the depositional sequences by accommodation space variations (Jervey, 1988) that can be either tectonic (vertical component of the lithosphere deformation) or eustatic (of tectonic or climatic origin). For the Cenozoic time interval studied, the eustatic variations are increasingly influenced by the climate over time, mainly after the Eocene-Oligocene transition, with the onset of an icehouse period and the growth of glaciers in Antarctica (e.g. Miller et al., 2008). Nevertheless, some authors, based on detailed subsidence analysis of well-dated basins, suggested that second order sequences are of tectonic origin, recording accelerating-decreasing variations in subsidence rates (e.g Vail et al. 1991). We

here use oxygen isotope curves of global deep ocean water compiled by Friedrich et al. (2012) and Zachos et al. (2001) as proxies of climate-induced eustasy for the Cretaceous and Cenozoic, respectively.

- **S8** sequence boundary (around the Santonian-Campanian boundary, i.e. 86.3 Ma) does not correspond to any major climatic cooling that might control a climatic eustatic fall at the origin of an unconformity (Friedrich et al., 2012). It is more likely the end of a cool period. However, the Late Cretaceous is a period of extremely long wavelength (several thousands of kilometres km) lithosphere deformation that is influenced by mantle dynamics (e.g. Nyblade and Robinson, 1994; Gurnis et al., 2000; De Wit,2007) that induced the major uplift phase of the South African Plateau. The uplift began around the Cenomanian-Turonian boundary (around 94 Ma) and ended in the Campanian (80-75 Ma) (Braun et al., 2014). A possible cause of this unconformity by uplift is reinforced by the thermochronological data, which indicate a major cooling event of the rocks on both sides of the Zambezi outlet: the southern portion of the Zimbabwe Plateau (Belton and Raab, 2010) to the west and the southern North Mozambique to the east (Emmel et al., 2011).

- **S7** sequence boundary (around the Cretaceous-Paleogene boundary, 67.3-63.2 Ma) is a regional-scale unconformity that extends throughout southern Africa and has a tectonic origin linked to the growth of the South African Plateau (Baby et al., 2018). However, its deformation processes are insufficiently understood. Eustatic origin cannot be inferred; the Cretaceous-Paleogene boundary is the onset of major warming and therefore major sea level rise (Friedrich et al., 2012).

- **S6** sequence boundary (late Thanetian to early Ypresian, 57.7-54.5 Ma), is marked by two carbonate platforms, the oldest is mixed siliciclastic (Upper Grudja Fm), while the youngest

contains only carbonates (Cheringoma Fm). Determining a tectonic origin is difficult, as there is no evidence of local or regional angular unconformity or a siliciclastic event. At the global scale, the uppermost Thanetian is a major period of sharp cooling (Zachos et al., 2001) before the PETM and the overall warming of the Ypresian Early Eocene Climatic Optimum. We suggest that the base S6 unconformity can be the eustatic decrease in sea level before the uppermost Thanetian cooling/low sea level.

- **S5** sequence boundary (latest Bartonian to early Priabonian, 38.2-36.2 Ma) corresponds to the initiation of the modern deltaic system of the Zambezi River. An unconformity occurring around the Eocene-Oligocene boundary has been characterized all around Africa and due to a major continent-scale uplift related to mantle dynamics (Burke and Gunnell, 2008). Nevertheless, because of its age (around the Eocene-Oligocene boundary) and wide occurrence at Africa-scale, its cause is debated and rather related to climatic and oceanographic changes (e.g. Séranne, 1999). Our age results indicate that this unconformity occurred before the Eocene-Oligocene climate change and therefore cannot be related to the associated major sea-level fall of approximately 100 m (Miller et al., 2008; de Boer et al., 2010). In the south-eastern portion of the South African Plateau along the Durban Basin and the Kwazulu-Maputaland Margin, Baby et al. (2018) identified on both stratigraphic and geomorphological evidences a continuous second uplift phase of the southern African Plateau from 40 Ma (early Bartonian) to 20 Ma (end of Burdigalian) with an unconformity at 26 Ma (Chattian) that may be the paroxysm of this uplift. We relate the unconformity, approximately of the same age given uncertainties in dating microfossils from cuttings, to this second uplift of the South African Plateau and the associated rejuvenation of the Zambezi

catchment to explain the siliciclastic supply and thus the formation of the modern Zambezi Delta.

- **S4** sequence boundary (late Chattian, 25-23 Ma) is related to the 26 Ma unconformity that Baby et al. (2018) identified in the Durban Basin and interpreted as the paroxysmal period of the second phase of the South African Plateau uplift.

- **S3** The base S3 sequence boundary (11.6 Ma, base of Tortonian) does not correspond to the major climate cooling in the second half of the Miocene that occurred during the Serravallian (around 13 Ma). It is related to the formation of the modern EARS, even though the timing of these events is not well dated (Macgregor, 2015; Simon et al., 2017).

- **S2** sequence boundary (5.6 Ma, uppermost Messinian) is both a major tectonic reorganization of the EARS and of the climate. From a climate viewpoint, this is a major humidification event, from drier to wetter conditions (Fig. 11; Bonnefille, 2010). The latest Miocene marks the formation of the Rukwa Rift and portions of the northern Malawi Rift. This is the end of the first phase of the Runkwe Volcanic Province (at the transition between the Rukwa and Malawi Rifts; Fontijn et al., 2012). This is a major change in the subsidence regime in the Albert Rift (Simon et al., 2017). This indicates a major reorganisation of drainage in the Malawi that likely extended far north before this event. It is difficult to assess what is due to lithosphere deformation vs. changes in precipitation; the latter most likely enhanced the former.

- **S1** sequence boundary (2.8 Ma, latest Piacenzian) is a period of lithosphere deformation and climate change. In the EARS, it corresponds to the paroxysmal phase of the Rungwe Volcanic Province (Fontijn et al., 2012) and, although it is unclear, the uplift of the northern

end of the Malawi Rift and an increase in subsidence to the south (Ebinger et al., 1993). From a climatic point of view this is the beginning of the glacial phases of the Pleistocene in the Northern Hemisphere (2.6 Ma). Again a climatically enhanced tectonic unconformity is the most probable.

5.2. The palaeoprecipitation record of the Zambezi Delta in the frame of the East African climate Cenozoic changes.

As already mentioned the palaeoprecipitation record of Africa is based mainly on local discontinuous outcrops of sediments dated with varying degrees of accuracy. This is also true for EARS sediments, in which the stratigraphic record consists of continental sediments interstratified within thick volcanic rocks. The only continuous records come from wells in the Aden Gulf (DSDP Site 261: Bonnefille, 2010) and offshore of Namibia (ODP site 1085; e.g. Dupont et al., 2011) in north-eastern and southern Africa, respectively.

The methods of palaeoprecipitation reconstructions are pollen assemblages, morphology of leaves (e.g. Jacobs, 2002), the structure of trunks (e.g. De Franceschi et al., 2016), the type of palaeosoils (e.g.Retallack et al., 2002) or are based on vertebrate associations (the number of herbivore fossils) or isotope geochemistry (the ratio between C3 proxy of woodlands vs. C4 proxy of grasslands). We here proposed a compilation (Fig. 11) of the palaeoprecipitation record of East Africa using both published data and our results offshore Zambezi Delta.

The Oligocene climate in Africa is not well known. In northern Africa, aridification is recorded around the Eocene-Oligocene boundary, with a change from a tropical forest (Eocene) to more arid conditions with dry or semi-arid forests (early Oligocene) (e.g. Louvet, 1973; Biondi et al., 1985). In Ethiopia (north of Lake Tana), late Oligocene flora and palaeosoils (Jacobs et al.,

2005; Pan et al., 2006) at that time a lowland setting indicate warm, humid conditions (precipitation greater than 1100 mm/yr). Southward along the Rukwa Rift, late Oligocene woods (Damblon et al., 1998, redated by Roberts et al., 2010) are typically tropical, with possible precipitation ranges from 1450-1750 mm/yr. These data indicating tropical warm and humid conditions during the late Oligocene in East Africa are confirmed by our data that suggests humid conditions along the Zambezi catchment during this time interval.

In Austral Africa (Atlantic side of Western Cape) palynological and biogeochemical studies indicate that in the early to middle Miocene, at the scale of astronomically driven climate change (Milankovitch cycles), alternating subtropical and warm temperate conditions occurred (Roberts et al., 2013) in an overall trend of cooler and drier conditions (Sciscio et al., 2016). Northward along the Atlantic Namibian Margin where the present day Namib Desert is located, the first evidence of aeolian sediments (Namib Desert) are dated from the late early Miocene (16 Ma; Pickford, 2014). Silicified wood and vertebrate fauna in the early Miocene Orange terraces (19-18 Ma, Burdigalian) suggest subtropical open woodlands (Neumann and Bamford, 2015). Isotopic studies of ratite eggshells preserved in aeolian sediments (Segalen et al., 2006) indicate homogeneous climate conditions during the Miocene, which was less arid than the present day and may have had winter precipitation. This aridification is related to the position of the Benguela Current and associated upwellings (Siesser, 1980; Diester-Haass et al., 1990). The offshore drilling record (ODP Site 1085) for the late Miocene indicates at least two phases of aridification: (1) a progressive change (Dupont et al., 2011) from 10-6 Ma (late Miocene), with the development of semi-arid succulent vegetation corresponding to modern Cape flora (i.e. fynbos), and (2) a second phase at 4.3 Ma (early Pliocene; Hoetzel et al., 2017). The early to middle Miocene aridification trend seems due to regional changes in southern Africa. The late

Miocene seems to be the first time that climate change differed between the Atlantic and Indian coasts of the southern African margins, with pervasive arid conditions in Namibia but a rapid return to more humid conditions in the Zambezi catchment.

In East Africa, north of the Kenyan Dome (Lokichar Basin) and around the Oligocene-Miocene boundary, palynological data (Vincens et al., 2006) suggest wet conditions (1200-1600 mm/yr) with a dry season in a mosaic of semi-deciduous forests and humid wood- lands. Later (early Miocene) and southward along the East African Dome around the Napak District (Uganda, 20.0-18.5 Ma; Pickford, 2002; Pickford et al., 2004) and Kisingiri Volcano (Kenyan portion of Lake Victoria; Bestland and Retallack, 1993; Collinson et al., 2009) the landscape is dominated by woodlands with small patches of rainforest. The main debate is the amount of grassland an indicator of seasonal aridity which seemed to exist based on palaeosoils and fauna (gastropods and vertebrates). Bestland and Retallack (1993) suggested that, based on palaeosoils, precipitation ranged from 550-750 mm/yr.

The middle Miocene climate experienced greater differences, most likely with alternating drier and wetter periods. In the Nyanza Rift, east of present day Lake Victoria, (Maboko Fm, around 15 Ma; Retallack et al. (2002) data on palaeosoils indicate dry environments, with precipitation ranging from 300-500 mm/yr. In the Kenyan Rift (Tugen Hills area), palaeobotanical data suggest relatively dry conditions around 13.3-12.0 Ma (Ngorora Fm, Rasmussen et al., 2017), with grassy savannah around 12.6 Ma (Kaberso Fm; Jacobs and Deino, 1996; Jacobs, 2002), followed by deciduous forests with precipitation from 955-1185 mm/yr, indicating more tropical conditions (rainforest; Jacobs and Kabuye, 1987). The main challenge is determining the local (e.g. topographic effect due to block tilting) or regional (dome-scale)

meaning of these drier and wetter events. Most authors agree that widespread aridification occurred from the early to middle Miocene in the East African Dome.

The late Miocene in the Kenyan Rift (eastern branch of the EARS) is characterised by a drier period followed by extreme humidification around 9.5 Ma (Samburu Hill - Suguta Valley; Sakai et al., 2010). In the Tugen Hills, the open vegetation structures in a climate with a pronounced dry season and precipitation of 490-610 mm/yr indicate that a drier period occurred around 9-10 Ma (Waril site; Jacobs, 2002). In the Tugen Hills in the late Miocene (Messinian), the presence of deciduous forest indicates more humid conditions (Kapturo site, 7.2-6.7 Ma, precipitation from 730-1020 mm/yr; Jacobs, 2002) and wet lowland rainforests (Mpesida Fm, 7-6 Ma; Kingston et al., 2002) or gallery forests similar to the modern Tana River (Mpesida Fm, 6.3 Ma; De Franceschi et al., 2016). The high lake levels around 7.2 Ma also indicate a humid period in the western branch of the EARS (Simon et al., 2017). In the Kenyan Rift (Tugen Hills), stable isotope analysis of herbivore teeth (Lukeino Fm; Roche et al., 2013) shows evidence of drier conditions around 6.1-5.8 Ma and wetter conditions around 5.7 and 5.3-4.5 Ma. This is in agreement with results from the Gulf of Aden (DSDP site 231; Bonnefille, 2010) that show maximum aridity around 5.9 Ma. The two humidity peaks characterized here around 11 ad 9.5-9 Ma in the Zambezi catchment might be related to the post 12 Ma and 9.5 Ma humidification identified in the Kenyan rift. The relative aridification around 10 Ma is in agreement with the drier even characterized by Jacobs (2002) in the Waril site.

6. Conclusion

(1) We have here developed an integrated method combining biostratigraphy, orbitostratigraphy and sequence stratigraphy in order to define a high resolution age model for the Zambezi Delta

and to discuss its main control parameters that are expected to be either climato-eustatic or tectonic.

- Although the biostratigraphic study was realised on cuttings, argues are strong for robust ages as information from calcareous nannofossils reinforced by planktonic foraminifera is almost constantly consistent. In addition, we coupled for the Neogene the biostratigraphy results with orbital stratigraphy (correlation of third order unconformities with Earth eccentricity cycles) using the calculated Earth orbital solution of Laskar.

- Three orders of sequences were defined: (1) seventeen third order sequences for Neogene times - Pl.0 to Pl.5 for the Pliocene-Pleistocene time span and M.1 to M.11 for the Miocene; (2) eight second order sequences from Late Cretaceous to Present; (3) one first order cycle subdivided into three steps, (an aggradational to retrogradational period during the Late Cretaceous, a mainly aggradational one until the middle Eocene, and a third prograding one corresponding to the Zambezi Delta initiation).

(2) From this stratigraphic framework we discussed the tectonic or climato-eustatic controls of the second-order sequences.

- Tectonic controlled sequences: S8 sequence boundary (dated around the Santonian-Campanian boundary, i.e. 86.3 Ma) is coeval with the uplift of the South African Plateau, S7 sequence boundary (dated around the Cretaceous-Paleogene boundary, 67.3-63.2 Ma), S5 sequence boundary (dated from the uppermost Bartonian to early Priabonian, 38.2-36.2 Ma) and S4 sequence boundary (ascribed to the late Chattian, 25-23 Ma) are consistent with the southern African Plateau periods of uplift, S3 sequence boundary (dated from the basal Tortonian, 11.6 Ma), S2 sequence boundary (dated 5.6 Ma, uppermost Messinian) and S1

sequence boundary (belonging to the latest Piacenzian, 2.8 Ma) are coeval to the EARS main periods of deformation and its southward propagation toward Mozambique.

- Climato-eustatic controlled sequences: S6 sequence boundary (dated from late Thanetian to early Ypresian, 57.7-54.5 Ma), S2 sequence boundary (dated from the latest Messinian, 5.6 Ma), S1 sequence boundary (attributed to the latest Piacenzian, 2.8 Ma) are consistent with worldwide climato-eustatic variations.

The Zambezi delta recorded both the uplifts of the South African Plateau, a major one during the Late Cretaceous (S8) and another one during the late Oligocene (S4). Later on, form the uppermost Miocene (S2) to today, the Zambezi delta is controlled by the southward propagation of the EAR.

(3) Analysis of pollen grains allowed defining a Humidity Index resulting in reconstruction of the precipitation record of the Zambezi catchment since 35 Ma. This index is defined as the pollen ratio tropical rain forest + warm-temperate semi-deciduous forest + pioneer forest / sparse forest to wooded savannah + dry grassland to open savannah, i.e. low altitude forest vegetation (humid context) vs. open vegetation (dry context).

The late Oligocene was a quite wet period getting dryer in the uppermost Chattian. No data are available for the early middle Miocene. The base Tortonian (11 Ma) - a humid peak - is in good agreement with the paleobotanical record in the Central Kenyan Rift System. The Messinian was a dry period with a slight increase of the humidity during the Zanclean and a sharp increase around the Zanclean-Piacenzian boundary.

Aknowledgments

This work was supported by the petroleum company TOTAL and the French oceanographic research agency IFREMER in the frame of the project PAMELA (Passive Margin Exploration Laboratory). All the data (seismic lines, well-logs and cuttings) were provided by TOTAL. We thank our colleagues of the PAMELA project for stimulating discussions. We also thank Brendan Simon for very helpful comments of the seismic interpretations.

We are very grateful to Marina Rabineau and to an anonymous reviewer for their critical comments that improved the early version of the manuscript.

References

Abreu, V., Neal, J., Bohacs, K., Kalbas, J. (eds.), 2011. Sequence stratigraphy of siliciclastic systems - The ExxonMobil methodology: An atlas of exercises. SEPM Concepts in Sedimentology and Paleontology 9, 226 p.

Baby, G., Guillocheau, F., Boulogne, C., Robin, C., Dall'Asta, M., 2018. Uplift history of a transform margin revealed by the stratigraphic record: The case of the Agulhas transform margin along the Southern African Plateau. Tectonophysics 731-732, 104-130.

Bardintzeff, J.M., Liégeois, J.P., Bonin, B., Bellon, H., Rasamimanana, G., 2010. Madagascar volcanic provinces linked to the Gondwana break-up: Geochemical and isotopic evidences for contrasting mantle sources. Gondwana Research 18 (2), 295–314.

Bartek, L.R., Vail, P.R., Anderson, J.B., Emmet, P.A., Wu, S., 1991. Effect of Cenozoic ice-sheet fluctuations in Antarctica on the stratigraphic signature of the Neogene. Journal of Geophysical Research 96 (B4), 6753–6778.

Bauer, F.U., Glasmacher, U., Ring, U., Grobe, R.W., Mambo, V., Starz, M., 2016. Long-term cooling history of the Albertine Rift: new evidence from the western rift shoulder, DR Congo. International Journal of Earth Sciences 105 (6), 1707–1728.

Beaudouin, C., Dennielou, B., Melki, T., Guichard, F., Kallel, N., Berné, S., Huchon, A., 2004. The Late Quaternary climatic signal recorded in a deep-sea turbiditic levee (Rhône Neofan, Gulf of Lions, NW Mediterranean): palynological constraints. Sedimentary Geology 172 (1), 85–97.

Beaudouin, C., Jouet, G., Suc, J.P., Berné, S., Escarguel, G., 2007a. Vegetation dynamics in southern France during the last 30 ky in the light of marine palynology. Quaternary Science Reviews 26 (7), 1037–1054.

Beaudouin, C., Suc, J.P., Acherki, N., Courtois, L., Rabineau, M., Aloïsi, J.C., Sierro, F.J., Oberlin, C., 2005a. Palynology of the northwestern Mediterranean shelf Gulf of Lions: First vegetational record for the last climatic cycle. Marine and Petroleum Geology 22 (6), 845–863.

Beaudouin, C., Suc, J. P., Cambon, G., Touzani, A., Giresse, P., Pont, D., Aloïsi, J.C., Marsset, T., Cochonat, P., Duzer, D., et al., 2005b. Present-day rhythmic deposition in the Grand Rhône prodelta (NW Mediterranean) according to high-resolution pollen analyses. Journal of Coastal Research, 292–306.

Beaudouin, C., Suc, J. P., Escarguel, G., Arnaud, M., Charmasson, S., 2007b. The significance of pollen signal in present-day marine terrigenous sediments: the example of the Gulf of Lions (western Mediterranean Sea). Geobios 40 (2), 159–172.

Belton, D.X., Raab, M.J., 2010. Cretaceous reactivation and intensified erosion in the Archean-Proterozoic Limpopo Belt, demonstrated by apatite fission track thermochronology. Tectonophysics 480 (1), 99–108.

Berggren, W.A., Kent, D.V., Swisher III, C.C., Aubry, M.P., 1995. A revised Cenozoic geochronology and chronostratigraphy. In: Berggren, W.A., Kent, D.V. Aubry, M.P., Hardenbol J. (eds.), Geochronology times scales and global stratigraphic correlation, SEPM Special Publication 54, 129-212.

Berggren, W.A., Pearson, P.N., 2005. A revised tropical to subtropical paleogene planktonic foraminiferal zonation. Journal of Foraminiferal Research 35 (4), 279–298.

Bestland, E., Retallack, G., 1993. Volcanically influenced calcareous palaeosols from the Miocene Kiahera Formation, Rusinga Island, Kenya. Journal of the Geological Society 150 (2), 293–310.

Biondi, E., Koeniguer, J.C., Privé-Gill, C., 1985. Bois fossiles et végétations arborescentes des régions méditerranéennes durant le Tertiaire. Plant Biosystem 119 (3-4), 167–196.

Bolli, H., Saunders, J., 1985. Oligocene to Holocene low latitude planktic foraminifera. In: Bolli, H.M, Saunders, J.B, Perch-Nielsen, K (eds.), Calcareous nannofossils biostratigraphy, Cambridge University Press, Cambridge, pp. 155–162.

Bonnefille, R., 2010. Cenozoic vegetation, climate changes and hominid evolution in tropical africa. Global and Planetary Change 72 (4), 390–41.

Boulila, S., Galbrun, B., Miller, K.G., Pekar, S.F., Browning, J.V., Laskar, J., Wright, J.D., 2011. On the origin of Cenozoic and Mesozoic third-order eustatic sequences. Earth-Science Reviews 109 (3), 94–112.

Braun, J., Guillocheau, F., Robin, C., Baby, G., Jelsma, H., 2014. Rapid erosion of the Southern African Plateau as it climbs over a mantle superswell. Journal of Geophysical Research: Solid Earth 119 (7), 6093–6112.

Brown, J., Fisher, W., 1977. Seismic-stratigraphic interpretation of depositional systems: Examples from Brazilian Rift and pull-apart basins. In: Payton, E. (ed.) Seismic stratigraphy – Applications to hydrocarbon exploration. American Association of Petroleum Geologists Memoir 26, pp. 213-248.

Burke, K., Gunnell, Y., 2008. The African erosion surface: a continental-scale synthesis of geomorphology, tectonics, and environmental change over the past 180 million years. Geological Society of America Memoirs 201, 1–66.

Burnet, J., 1998. Upper Cretaceous. In: Brown, P.R. (Ed.) Plankton stratigraphy, Chapman and Hall, London, pp. 132–199.

Cambon, G., Suc, J.P., Aloisi, J.C., Giresse, P., Monaco, A., Touzani, A., Duzer, D., Ferrier, J., 1997. Modern pollen deposition in the Rhône delta area (lagoonal and marine sediments), France. Grana 36 (2), 105–113.

Cathro, D.L., Austin Jr., J.A., Moss, G.D., 2003. Progradation along a deeply submerged Oligocene–Miocene heterozoan carbonate shelf: How sensitive are clinoforms to sea level variations? American Association of Petroleum Geologists Bulletin 87, 1547–1574.

Catuneanu, O., Abreu, V., Bhattacharya, J., Blum, M., Dalrymple, R., Eriksson, P., Fielding, C.R., Fisher, W., Galloway, W., Gibling, M. et al., 2009. Towards the standardization of sequence stratigraphy. Earth-Science Reviews 92 (1), 1–33.

Chesters, K.I., 1957. The Miocene flora of Rusinga Island, Lake Victoria, Kenya. Palaeontographica Abteilung B, 30–71.

Chorowicz, J., 2005. The east African rift system. Journal of African Earth Sciences 43 (1), 379–410.

Cochran, J. R., 1988. Somali Basin, Chain Ridge, and origin of the Northern Somali Basin gravity and geoid low. Journal of Geophysical Research: Solid Earth 93 (B10), 11985–12008.

Cohen, A. S., Soreghan, M. J., Scholz, C. A., 1993. Estimating the age of formation of lakes: an example from Lake Tanganyika, East African Rift system. Geology 21 (6), 511–514.

Collinson, M.E., Andrews, P., Bamford, M.K., 2009. Taphonomy of the early Miocene flora, Hiwegi Formation, Rusinga Island, Kenya. Journal of Human Evolution 57 (2), 149–162.

Coulié, E., Quidelleur, X., Gillot, P.Y., Courtillot, V., Lefevre, J.C., Chiesa, S., 2003. Comparative K-Ar and Ar/Ar dating of Ethiopian and Yemenite Oligocene volcanism: implications for timing and duration of the Ethiopian traps. Earth and Planetary Science Letters 206 (3), 477–492.

Cour, P., Duzer, D., 1978. La signification climatique, édaphique et sédimentologique des rapports entre taxons en analyse pollinique. Annales des Mines de Belgique. (7-8), 155–164.

Courgeon, S., Jorry, S., Camoin, G., BouDagher-Fadel, M., Jouet, G., Révillon, S., Bachèlery, P., Pelleter, E., Borgomano, J., Poli, E., et al., 2016. Growth and demise of Cenozoic isolated carbonate platforms: New insights from the Mozambique Channel seamounts (SW Indian Ocean). Marine Geology 380, 90–105.

Dalibard, M., Popescu, S.M., Maley, J., Baudin, F., Melinte-Dobrinescu, M.C., Pittet, B., Marsset, T., Dennielou, B., Droz, L., Suc, J.P., 2014. High-resolution vegetation history of West Africa during the last 145 ka. Geobios 47 (4), 183–198.

Damblon, F., Gerrienne, P., d'Outrelepont, H., Delvaux, D., Beeckman, H., Back, S., 1998. Identification of a fossil wood specimen in the Red Sandstone Group of south-western Tanzania: stratigraphical and tectonic implications. Journal of African Earth Sciences 26 (3), 387–396.

Daszinnies, M., 2006. The Phanerozoic thermo-tectonic evoultion of northern Mozambique constrained by fission track and (U-Th)/He analyses. Ph.D. thesis, University of Bremen.

de Boer, B., Van de Wal, R., Bintanja, R., Lourens, L., Tuenter, E., 2010. Cenozoic global ice-volume and temperature simulations with 1-D ice-sheet models forced by benthic $\delta^{18}O$ records. Annals of Glaciology 51 (55), 23–33.

De Franceschi, D., Bamford, M., Pickford, M., Senut, B., 2016. Fossil wood from the upper Miocene Mpesida Beds at Cheparain (Baringo District, Kenya): Botanical affinities and palaeoenvironmental implications. Journal of African Earth Sciences 115, 271–280.

De Schepper, S., Gibbard, P.L., Salzmann, U., Ehlers, J., 2014. A global synthesis of the marine and terrestrial evidence for glaciation during the Pliocene Epoch. Earth-Science Reviews 135, 83–102.

De Wit, M., 2007. The Kalahari Epeirogeny and climate change: differentiating cause and effect from core to space. South African Journal of Geology 110 (2-3), 367–392.

DeBusk, G.H., 1997. The distribution of pollen in the surface sediments of Lake Malawi, Africa, and the transport of pollen in large lakes. Review of Palaeobotany and Palynology 97 (1-2), 123–153.

deMenocal, P.B., 1995. Plio-Pleistocene African climate. Science, 53–59.

Diester-Haass, L., Meyers, P.A., Rothe, P., 1990. Miocene history of the Benguela Current and Antarctic ice volumes: Evidence from rhythmic sedimentation and current growth across the Walvis Ridge (Deep Sea Drilling Project Sites 362 and 532). Paleoceanography 5 (5), 685–707.

Du Toit, A., 1933. Crustal movement as a factor in the geographical evolution of South Africa. South African Geographical Journal 16 (3), 2-20.

Dupont, L.M., Linder, H.P., Rommerskirchen, F., Schefuss, E., 2011. Climate-driven rampant speciation of the Cape flora. Journal of Biogeography 38 (6), 1059–1068.

Ebinger, C., 1989. Tectonic development of the western branch of the East African rift system. Geological Society of America Bulletin 101 (7), 885–903.

Ebinger, C., Deino, A., Tesha, A., Becker, T., Ring, U., 1993. Tectonic controls on rift basin morphology: evolution of the Northern Malawi (Nyasa) Rift. Journal of Geophysical Research: Solid Earth 98 (B10), 17821–17836.

Emmel, B., Kumar, R., Jacobs, J., Ueda, K., Van Zuilen, M., Matola, R., 2014. The low-temperature thermochronological record of sedimentary rocks from the central Rovuma Basin (N Mozambique) – Constraints on provenance and thermal history. Gondwana Research 25, 1216-1229.

Faugères, J.C., Stow, D.A., Imbert, P., Viana, A., 1999. Seismic features diagnostic of contourite drifts. Marine Geology 162 (1), 1–38.

Feakins, S. J., Levin, N. E., Liddy, H. M., Sieracki, A., Eglinton, T. I., Bonnefille, R., 2013. Northeast African vegetation change over 12 my. Geology 41 (3), 295–298.

Flores, G., 1973. The Cretaceous and Tertiary sedimentary basins of Mozambique and Zululand. In: Sedimentary basins of the African coasts, Association of African Geological Surveys, Paris, pp. 81–111.

Fontijn, K., Williamson, D., Mbede, E., Ernst, G.G., 2012. The Rungwe Volcanic Province, Tanzania - A volcanological review. Journal of African Earth Sciences 63,12–31.

Friedrich, O., Norris, R. D., Erbacher, J., 2012. Evolution of middle to Late Cretaceous oceans - a 55 my record of Earth's temperature and carbon cycle. Geology 40 (2), 107–110.

Gallagher, K., Brown, R., 1999. The Mesozoic denudation history of the Atlantic margins of southern Africa and southeast Brazil and the relationship to offshore sedimentation. Geological Society, London, Special Publications 153 (1), 41–53.

Goodlad, S., Martin, A., Hartnady, C., 1982. Mesozoic magnetic anomalies in the southern Natal Valley. Nature 295 (5851), 686–688.

Graciansky, P.C. de, Hardenbol, J., Jacquin, T., Vail, P.R., 1998. Mesozoic and Cenozoic sequence stratigraphy of European Basins. SEPM Special Publication, 60, 786 p.

Gradstein, F. M., Ogg, J. G., Schmitz, M., Ogg, G., 2012. The geologic time scale 2012. Elsevier, Amsterdam, 1144 p.

Greenlee, S.M., Moore, T.C., 1988. Recognition and interpretation of depositional sequences and calculations of sea level changes from stratigraphic data-offshore New Jersey and Alabama Tertiary. In: Wilgus, C.K., Hastings, B.S., Kendall, C.G.St.C., Posamentier, H.W., Ross, C.A., Van Wagoner, J.C. (Eds.), Sea Level Changes: An Integrated Approach. SEPM Special Publications 42, pp. 329–353.

Guillocheau, F., Rouby, D., Robin, C., Helm, C., Rolland, N., Le Carlier de Veslud, C., Braun, J., 2012. Quantification and causes of the terrigeneous sediment budget at the scale of a continental margin: a new method applied to the Namibia-South Africa margin. Basin Research 24 (1), 3–30.

Gurnis, M., Mitrovica, J.X., Ritsema, J., van Heijst, H.J., 2000. Constraining mantle density structure using geological evidence of surface uplift rates: The case of the African superplume. Geochemistry, Geophysics, Geosystems 1 (7) 1999GC000035.

Hansen, J., Sato, M., Russell, G., Kharecha, P., 2013. Climate sensitivity, sea level and atmospheric carbon dioxide. Philosophical Transactions of the Royal Society A371, 20120294.

Helland-Hansen, W., Gjelberg, J.G., 1994. Conceptual basis and variability in sequence stratigraphy: a different perspective. Sedimentary Geology 92 (1-2), 31–52.

Helland-Hansen, W., Hampson, G., 2009. Trajectory analysis: concepts and applications. Basin Research 21 (5), 454–483.

Helland-Hansen, W., Martinsen, O.J., 1996. Shoreline trajectories and sequences: description of variable depositional-dip scenarios. Journal of Sedimentary Research 66 (4), 567-585.

Herendeen, P.S., Jacobs, B.F., 2000. Fossil legumes from the middle Eocene (46.0 Ma) Mahenge flora of Singida, Tanzania. American Journal of Botany 87 (9), 1358–1366.

Hoetzel, S., Dupont, L.M., Marret, F., Jung, G., Wefer, G., 2017. Steps in the intensification of Benguela upwelling over the Walvis Ridge during Miocene and Pliocene. International Journal of Earth Sciences 106 (1), 171–183.

Hunt, D., Tucker, M.E., 1992. Stranded parasequences and the forced regressive wedge systems tract: deposition during base-level fall. Sedimentary Geology 81 (1-2), 1–9.

Jacobs, B.F., 2002. Estimation of low-latitude paleoclimates using fossil angiosperm leaves: examples from the Miocene Tugen Hills, Kenya. Paleobiology 28 (3), 399–421.

Jacobs, B.F., Deino, A.L., 1996. Test of climate-leaf physiognomy regression models, their application to two Miocene floras from Kenya, and $^{40}Ar/^{39}Ar$ dating of the Late Miocene Kapturo site. Palaeogeography, Palaeoclimatology, Palaeoecology 123 (1-4), 259–271.

Jacobs, B.F., Herendeen, P.S., 2004. Eocene dry climate and woodland vegetation in trop- ical Africa reconstructed from fossil leaves from northern Tanzania. Palaeogeography, Palaeoclimatology, Palaeoecology 213 (1), 115–123.

Jacobs, B.F., Kabuye, C.H., 1987. A middle Miocene (12.2 my old) forest in the East African Rift Valley, Kenya. Journal of Human Evolution 16 (2), 147–155.

Jacobs, B.F., Pan, A.D., Scotese, C.R., 2010. A review of the Cenozoic vegetation history of Africa. In: Werdelin, L., Sanders, W.J. (eds.) Cenozoic mammals of Africa, University of California Press, Berkeley, pp. 57–72.

Jacobs, B. F., Tabor, N., Feseha, M., Pan, A., Kappelman, J., Rasmussen, T., Sanders, W., Wiemann, M., Crabaugh, J., Massini, J. G., 2005. Oligocene terrestrial strata of northwestern Ethiopia: a preliminary report on paleoenvironments and paleontology. Palaeontologia electronica, 8 (1), 25A:19 p.

Jacobs, B.F., Winkler, D.A., 1992. Taphonomy of a middle Miocene autochthonous forest assemblage, Ngorora Formation, central Kenya. Palaeogeography, Palaeoclimatology, Palaeoecology 99 (1-2), 31–40.

Jelsma, H.A., De Wit, M.J., Thiart, C., Dirks, P.H., Viola, G., Basson, I.J., Anckar, E., 2004. Preferential distribution along transcontinental corridors of kimberlites and related rocks of Southern Africa. South African Journal of Geology 107 (1-2), 301–324.

Jervey, M.T., 1988. Quantitative geological modeling of siliciclastic rock sequences and their seismic expression. In: Wilgus, C.K., Hastings, B.S., Kendall, C.G.St.C., Posamentier, H.W., Ross, C.A., Van Wagoner, J.C. (eds.), Sea level changes: An integrated approach, SEPM Special Publication 42, pp. 47 -69.

Jokat, W., Boebel, T., Knig, M., Meyer, U., 2003. Timing and geometry of early Gondwana breakup. Journal of Geophysical Research: Solid Earth 108 (B9), 2428.

Kingston, J.D., Jacobs, B.F., Hill, A., Deino, A., 2002. Stratigraphy, age and environments of the late Miocene Mpesida Beds, Tugen Hills, Kenya. Journal of Human Evolution 42 (1-2), 95–116.

Konig, M., Jokat, W., 2010. Advanced insights into magmatism and volcanism of the Mozambique Ridge and Mozambique Basin in the view of new potential field data. Geophysical Journal International 180 (1), 158–180.

Lafourcade, P., 1984. Etude géologique et géophysique de la marge continentale du sud Mozambique (17°S à 28°S). Ph.D. thesis, Université Paris 6.

Laskar, J., Fienga, A., Gastineau, M., Manche, H., 2011. La2010: a new orbital solution for the long-term motion of the Earth. Astronomy & Astrophysics 532, A89.

Laskar, J., Robutel, P., Joutel, F., Gastineau, M., Correia, A., Levrard, B., 2004. A long-term numerical solution for the insolation quantities of the Earth. Astronomy & Astrophysics 428 (1), 261–285.

Leinweber, V.T., Jokat, W., 2011. Is there continental crust underneath the northern Natal Valley and the Mozambique Coastal Plains? Geophysical Research Letters 38 (14), L14303.

Leinweber, V.T., Jokat, W., 2012. The Jurassic history of the Africa - Antarctica corridor - new constraints from magnetic data on the conjugate continental margins. Tectonophysics 530, 87–101.

Leinweber, V.T., Klingelhoefer, F., Neben, S., Reichert, C., Aslanian, D., Matias, L., Heyde, I., Schreckenberger, B., Jokat, W., 2013. The crustal structure of the Central Mozambique continental margin - Wide angle seismic, gravity and magnetic study in the Mozambique Channel, Eastern Africa. Tectonophysics 599, 170–196.

Louvet, P., 1973. Contribution à l'étude de la mise en place des forêts tropicales africaines. Comptes Rendus des Séances de la Société de Biogéographie 431, 81-86.

Macgregor, D., 2015. History of the development of the East African Rift System: a series of interpreted maps through time. Journal of African Earth Sciences 101, 232–252.

MacPhee, D., 2006. Exhumation, rift-flank uplift, and the thermal evolution of the Rwenzori Mountains determined by combined (U-Th)/He and U-Pb thermochronometry. Ph.D. thesis, Massachusetts Institute of Technology.

Mahoney, J., Duncan, R., Khan, W., Gnos, E., McCormick, G., 2002. Cretaceous volcanic rocks of the south Tethyan suture zone, Pakistan: implications for the Réunion hotspot and Deccan traps. Earth and Planetary Science Letters 203 (1), 295–310.

Martinez, M., Dera, G., 2015. Orbital pacing of carbon fluxes by a 9 My eccentricity cycle during the Mesozoic. Proceedings of the National Academy of Sciences 112 (41), 12604–12609.

Martini, E., 1971. Standard tertiary and quaternary calcareous nannoplankton zonation. In: Farinacci, A. (ed.), Proceedings of the second Planktonic Conference, Roma 1970, 2, pp. 739–785.

Miller, K., Wright, J., Katz, M., Browning, J., Cramer, B., Wade, B.S., Mizintseva, S., 2008. A view of Antarctic ice-sheet evolution from sea-level and deep-sea isotope changes during the Late Cretaceous - Cenozoic. In: Cooper, A.K., Barrett, P.J., Stagg, H., Storey, B., Stump, E., Wise, W., and the 10th ISAES editorial team (eds.), Antarctica: A keystone in a changing world, Proceedings of the 10th International Symposium on Antarctic Earth Sciences, Washington, DC, The National Academies Press, pp. 55-70.

Miller, K.G., Mountain, G.S., Wright, J.D., Browning, J.V., 2011. A 180-million-year record of sea level and ice volume variations from continental margin and deep-sea isotopic records. Oceanography 24(2), 40–53.

Milliman, J.D., Syvitski, J.P., 1992. Geomorphic/tectonic control of sediment discharge to the ocean: the importance of small mountainous rivers. The Journal of Geology 100 (5), 525–544.

Mitchum, R.M. Jr, Vail, P.R., Thompson, S. III, 1977. Seismic stratigraphy and global changes of sea level: Part 2. The depositional sequence as a basic unit for stratigraphic analysis. In: Payton, E. (ed.) Seismic stratigraphy – Applications to hydrocarbon exploration. American Association of Petroleum Geologists Memoir 26, pp. 53-62.

Moore, A., 1999. A reappraisal of epeirogenic flexure axes in southern Africa. South African Journal of Geology 102 (4), 363–376.

Moore, A., Larkin, P., 2001. Drainage evolution in south-central Africa since the breakup of Gondwana. South African Journal of Geology 104 (1), 47–68.

Moore, A.E., Cotterill, F.P., Main, M.P., Williams, H.B., 2007. The Zambezi River. In: Gupta, A. (ed.), Large rivers: geomorphology and management, John Wiley & Sons Ltd, New-York, pp. 311–332.

Morley, R., 2011. Cretaceous and Tertiary climate change and the past distribution of megathermal rainforests. In: Tropical rainforest responses to climatic change. Springer, pp. 1–34.

Mougenot, D., Recq, M., Virlogeux, P., Lepvrier, C., 1986. Seaward extension of the East African Rift. Nature 321 (6070), 599–603.

Mueller, C.O., Jokat, W., Schreckenberger, B., 2016. The crustal structure of Beira High, central Mozambique - Combined investigation of wide-angle seismic and potential field data. Tectonophysics 683, 233–254.

Nairn, A.E., Lerche, I., Iliffe, J. E., 1991. Geology, basin analysis, and hydrocarbon potential of Mozambique and the Mozambique Channel. Earth-Science Reviews 30 (1), 81–123.

Neal, J., Abreu, V., 2009. Sequence stratigraphy hierarchy and the accommodation succession method. Geology 37, 779–782.

Neumann, F.H., Bamford, M.K., 2015. Shaping of modern southern African biomes: Neogene vegetation and climate changes. Transactions of the Royal Society of South Africa 70 (3), 195–212.

Nugent, C., 1990. The Zambezi River: tectonism, climatic change and drainage evolution. Palaeogeography, Palaeoclimatology, Palaeoecology 78 (1-2), 55–69.

Nyblade, A.A., Robinson, S.W., 1994. The African Superswell. Geophysical research letters 21 (9), 765–768.

Olsson, R., Hemleben, C., Berggren, W., Huber, B., 1999. Atlas of Paleocene planktonic foraminifera. In: Smithsonian Contributions to Paleobiology. pp. 85–252.

Pan, A.D., Jacobs, B.F., Dransfield, J., Baker, W. J., 2006. The fossil history of palms (Arecaceae) in Africa and new records from the late Oligocene (28 - 27 Mya) of north- western Ethiopia. Botanical Journal of the Linnean Society 151 (1), 69–81.

Pearson, P., Olson, R., Huber, B., Hemleben, C., Berggren, W., 2006. Atlas of Eocene planktonic foraminifera. Cushman Foundation Spec. Publ 41, 514 p.

Pekkala, Y., Kuivasaari, T., Gonalves, R., Deus, M., Chaque, F., Almeida, C., 2008. Review of industrial minerals in Mozambique. Geol. Surv. Finland, Spec. Pap 48, 289–306.

Perch-Nielsen, K., 1985a. Cenozoic calcareous nannofossils. In: Plankton stratigraphy, Bolli, H.M., Saunders, J.B., Perch-Nielsen, K Edition. Cambridge University press, Cambridge, pp. 427–554.

Perch-Nielsen, K., 1985b. Mesozoic calcareous nannofossils. In: Bolli, H.M., Saunders, J.B., Perch-Nielsen, K (eds.), Plankton stratigraphy, Cambridge University Press, Cambridge, pp. 329–426.

Pickford, M., 2002. Early Miocene grassland ecosystem at Bukwa, Mount Elgon, Uganda. Comptes Rendus Palevol 1 (4), 213–219.

Pickford, M., 2014. New Ratite eggshells from the Miocene of Namibia. Communications of the Geological Survey of Namibia 15, 70–90.

Pickford, M., Senut, B., Mourer-Chauvire, C., 2004. Early Pliocene Tragulidae and peafowls in the Rift Valley, Kenya: evidence for rainforest in East Africa. Comptes Rendus Palevol 3 (3), 179–189.

Pik, R., Marty, B., Carignan, J., Lave, J., 2003. Stability of the Upper Nile drainage network (Ethiopia) deduced from (U-Th)/He thermochronometry: implications for uplift and erosion of the Afar plume dome. Earth and Planetary Science Letters 215 (1), 73–88.

Pik, R., Marty, B., Carignan, J., Yirgu, G., Ayalew, T., 2008. Timing of East African Rift development in southern Ethiopia: Implication for mantle plume activity and evolution of topography. Geology 36 (2), 167–170.

Plint, A.G., 1988. Sharp-base shoreface sequences and" offshore bars" in the Cardium Formation of Alberta: their relationship to relative changes in sea-level. In: Wilgus, C.K., Hastings, B.S., Kendall, C.G.St.C., Posamentier, H.W., Ross, C.A., Van Wagoner, J.C. (eds.), Sea level changes: An integrated approach, SEPM Special Publication 42, pp. 357–370.

Plint, A.G., Nummedal, D., 2000. The falling stage systems tract: recognition and im- portance in sequence stratigraphic analysis. Geological Society, London, Special Publications 172 (1), 1–17.

Plummer, P.S., Belle, E., 1995. Mesozoic tectono-stratigraphic evolution of the Seychelles microcontinent. Sedimentary Geology 96 (1-2), 73–91.

Posamentier, H.W., Vail, P.R., 1988. Eustatic controls on clastic deposition II - sequence and systems tract models. In: Wilgus, C.K., Hastings, B.S., Kendall, C.G.St.C., Posamentier, H.W., Ross, C.A., Van Wagoner, J.C. (eds.), Sea level changes: An integrated approach, SEPM Special Publication 42, pp. 125-154.

Poumot, C., 1989. Palynological evidence for eustatic events in the tropical neogene. Bul- letin des Centres de Recherches Exploration-Production Elf Aquitaine 13 (2), 437–453.

Prescott, C.L., Haywood, A.M., Dolan, A.M., Hunter, S.J., Pope, J.O., Pickering, S.J., 2014. Assessing orbitally-forced interglacial climate variability during the mid-Pliocene Warm Period. Earth and Planetary Science Letters 400, 261–271.

Raffi, I., Backman, J., Fornaciari, E., Pälike, H., Rio, D., Lourens, L., Hilgen, F., 2006. A review of calcareous nannofossil astrobiochronology encompassing the past 25 million years. Quaternary Science Reviews 25 (23), 3113–3137.

Raillard, S., 1990. Les marges de l'Afrique de l'Est et les zones de fracture associées: Chaine Davie et Ride du Mozambique. Ph.D. thesis, Université Pierre et Marie Curie, Paris.

Rasmussen, C., Reichenbacher, B., Lenz, O., Altner, M., Penk, S.B., Prieto, J., Bruesch, D., 2017. Middle - late Miocene palaeoenvironments, palynological data and a fossil fish Lagerstatte from the Central Kenya Rift (East Africa). Geological Magazine 154 (1), 24–56.

Rebesco, M., Hernandez-Molina, F.J., Van Rooij, D., Wahlin, A., 2014. Contourites and associated sediments controlled by deep-water circulation processes: state-of-the-art and future considerations. Marine Geology 352, 111–154.

Retallack, G.J., Wynn, J.G., Benefit, B.R., McCrossin, M.L., 2002. Paleosols and paleoenvironments of the middle Miocene, Maboko Formation, Kenya. Journal of Human Evolution 42 (6), 659–703.

Roberts, D.L., Sciscio, L., Herries, A.I., Scott, L., Bamford, M.K., Musekiwa, C., Tsikos, H., 2013. Miocene fluvial systems and palynofloras at the southwestern tip of Africa: Implications for regional and global fluctuations in climate and ecosystems. Earth-science reviews 124, 184–201.

Roberts, E.M., OConnor, P.M., Stevens, N.J., Gottfried, M.D., Jinnah, Z.A., Ngasala, S., Choh, A. M., Armstrong, R.A., 2010. Sedimentology and depositional environments of the Red Sandstone Group, Rukwa Rift Basin, southwestern Tanzania: New insight into Cretaceous and Paleogene terrestrial ecosystems and tectonics in sub-equatorial Africa. Journal of African Earth Sciences 57 (3), 179–212.

Roche, D., Segalen, L., Senut, B., Pickford, M., 2013. Stable isotope analyses of tooth enamel carbonate of large herbivores from the Tugen Hills deposits: Palaeoenvironmental context of the earliest Kenyan hominids. Earth and Planetary Science Letters 381, 39–51.

Sakai, T., Saneyoshi, M., Tanaka, S., Sawada, Y., Nakatsukasa, M., Mbua, E., Ishida, H., 2010. Climate shift recorded at around 10 Ma in Miocene succession of Samburu Hills, northern Kenya Rift, and its significance. Geological Society, London, Special Publications 342 (1), 109–127.

Salman, G., Abdula, I., 1995. Development of the Mozambique and Ruvuma sedimentary basins, offshore Mozambique. Sedimentary Geology 96 (1), 7–41.

Sciscio, L., Tsikos, H., Roberts, D., Scott, L., van Breugel, Y., Damste, J.S., Schouten, S., Grocke, D., 2016. Miocene climate and vegetation changes in the Cape Peninsula, South Africa: evidence from biogeochemistry and palynology. Palaeogeography, Palaeoclimatology, Palaeoecology 445, 124–137.

Scotese, C., Boucot, A., McKerrow, W., 1999. Gondwanan palaeogeography and palaeo-climatology. Journal of African Earth Sciences 28 (1), 99–114.

Segalen, L., Renard, M., Lee-Thorp, J. A., Emmanuel, L., Le Callonnec, L., De Raflis, M., Senut, B., Pickford, M., Melice, J.-L., 2006. Neogene climate change and emergence of C4 grasses in

the Namib, southwestern Africa, as reflected in ratite ^{13}C and ^{18}O. Earth and Planetary Science Letters 244 (3), 725–734.

Sépulchre, P., Ramstein, G., Fluteau, F., Schuster, M., Tiercelin, J.J., Brunet, M., 2006. Tectonic uplift and Eastern Africa aridification. Science 313 (5792), 1419–1423.

Séranne, M., 1999. Early Oligocene stratigraphic turnover on the west Africa continental margin: a signature of the Tertiary greenhouse-to-icehouse transition? Terra Nova- Oxford 11 (4), 135–140.

Siesser, W. G., 1980. Late Miocene origin of the Benguela upswelling system off northern Namibia. Science 208 (4441), 283–285.

Simon, B., Guillocheau, F., Robin, C., Dauteuil, O., Nalpas, T., Pickford, M., Senut, B., Lays, P., Bourges, P., Bez, M., 2017. Deformation and sedimentary evolution of the Lake Albert Rift (Uganda, East African Rift System). Marine and Petroleum Geology 86, 17–37.

Storey, M., Mahoney, J.J., Saunders, A.D., Duncan, R.A., Kelley, S.P., Coffin, M.F., et al., 1995. Timing of hot spot-related volcanism and the breakup of Madagascar and India. Science 267, 852–852.

Strasser, A., Hillgrtner, H., Hug, W., Pittet, B., 2000. Third-order depositional sequences reflecting Milankovitch cyclicity. Terra Nova 12 (6), 303–311.

Suc, J.P., Fauquette, S., Popescu, S.M., 2004. L'investigation palynologique du Cénozoïque passe par les herbiers. In: Actes du Colloque « Les herbiers: un outil d'avenir. Tradition et modernité », Villeurbanne. Association française pour la Conservation des Espèces Végétales, Nancy. pp. 67–87.

Thomas, D.S., Shaw, P.A., 1988. Late Cenozoic drainage evolution in the Zambezi Basin: geomorphological evidence from the Kalahari rim. Journal of African Earth Sciences 7 (4), 611–618.

Tiedemann, R., Sarnthein, M., Shackleton, N.J., 1994. Astronomic timescale for the Pliocene Atlantic $\delta^{18}O$ and dust flux records of Ocean Drilling Program Site 659. Paleoceanography 9 (4), 619–638.

Tikku, A.A., Marks, K.M., Kovacs, L.C., 2002. An Early Cretaceous extinct spreading center in the northern Natal Valley. Tectonophysics 347 (1), 87–108.

Timberlake, J., 2000. Biodiversity of the Zambezi basin. Biodiversity Foundation for Africa, Bulawayo (Zimbabwe), Occasional Publications in Biodiversity, 9, 23 p.

Trauth, M.H., Maslin, M.A., Deino, A., Strecker, M.R., 2005. Late Cenozoic moisture history of East Africa. Science 309 (5743), 2051–2053.

Vail, P., Audemard, F., Bowman, S.A., Eisner, P.N., Perez-Cruz, C., 1991. The stratigraphic signatures of tectonics, eustacy and sedimentology - an overview. In: Einsele, G., Ricken, W., Seilacher, A. (eds.), Cycles and events in stratigraphy, Springer-Verlag, Berlin, pp. 617–659.

Vail, P.R., Mitchum R.M. Jr, Thompson, S. III, 1977. Seismic stratigraphy and global changes of sea level: Part 3. Relative changes of sea level from Coastal Onlap. In: Payton, E. (ed.) Seismic stratigraphy – Applications to hydrocarbon exploration. American Association of Petroleum Geologists Memoir 26, pp. 63-82.

Van der Beek, P., Summerfield, M.A., Braun, J., Brown, R.W., Fleming, A., 2002. Modeling post-breakup landscape development and denudational history across the southeast African

(Drakensberg Escarpment) margin. Journal of Geophysical Research: Solid Earth 107 (B12), ETG11.

Vincens, A., Tiercelin, J.J., Buchet, G., 2006. New Oligocene - early Miocene microflora from the southwestern Turkana Basin: Palaeoenvironmental implications in the northern Kenya Rift. Palaeogeography, Palaeoclimatology, Palaeoecology 239 (3), 470–486.

Virlogeux, P., 1987. Géologie de la marge nord-mozambique et de la chaine de Davie (9°S à 21°S): campagne md40-Macamo. Ph.D thesis, Université Paris 6.

Woolley, A., 1987. Lithosphere metasomatism and the petrogenesis of the Chilwa Province of alkaline igneous rocks and carbonatites, Malawi. Journal of African Earth Sciences 6 (6), 891–898.

Young, J., 1998. Neogene. In: Bown, P.R. (ed.), Calcareous Nannofossils Biostratigraphy, British Micropaleontological Society Publications Series, Chapman and Hall, London, 8, pp. 225–265.

Zachos, J., Pagani, M., Sloan, L., Thomas, E., Billups, K., 2001. Trends, rhythms, and aberrations in global climate 65 Ma to present. Science 292 (5517), 686–693.

Zeeden, C., Hilgen, F., Westerhold, T., Lourens, L., Röhl, U., Bickert, T., 2013. Revised Miocene splice, astronomical tuning and calcareous plankton biochronology of ODP Site 926 between 5 and 14.4 Ma. Palaeogeography, Palaeoclimatology, Palaeoecology 369, 430–451.

Figures and supplementary materials

Figures

Fig. 1: The Zambezi sedimentary system. A: Location in Austral Africa (catchment) and in the Mozambique Channel (deep-sea fan). B: Main geological features of the catchment (Cenozoic Kalahari Basin, Late Carboniferous to Triassic Karoo rifts, Neogene rifts and main faults).

Fig. 2: Summary chart of approaches used to interpret seismic stratigraphy.

Fig. 3: Present day vegetation distribution within the Zambezi catchment (Timberlake, 2000).

Fig. 4: Summary chart of the main geodynamic (oceanic accretion, plumes, volcanism) and tectonic (main African and Mozambican deformations, denudations and uplifts) events with the stratigraphy (lithostratigraphy and main sequence boundaries and marine floodings) from the literature.

Fig. 5: Margin delta depositional profile: environments and lithology, clinoforms height and main seismic facies.

Fig. 6: Zambezi Delta regional seismic line from the upstream coastal plain bordered by the Cheringoma Plateau to the Beira High (see location on Fig. 1B): age model and

sedimentary environments.

Fig. 7: Studied wells (see location on Fig. 1B): lithology from well-logs and cuttings, sequence boundary (Uc) in the second order sequences (labelled S1 to S8 from the number in the above sequence) and biostratigraphic dataset (calcareous nannofossils and planktonic foraminifers).

Fig. 8: Biostratigraphy of Well X1. The grey stripes show the proposed correlations of the studied samples with the occurrence charts of calcareous nannofossil and/or planktonic foraminifer biostratigraphic markers and relative biozones.

Fig. 9: Biostratigraphy of Well X3. The grey stripes show the proposed correlations of the studied samples with the occurrence charts of calcareous nannofossil and/or planktonic foraminifer biostratigraphic markers and relative biozones.

Fig. 10: Age model for Zambezi Delta Neogene sediments: (1) repetitive unconformity-bounded third-order depositional sequences influenced by climate-induced sea level changes, defined on both offlap break migration and stratigraphic truncations (labelled from Pl.0 to Pl.5 and M.1 to M.11) and (2) calibration of the third-order sequence boundaries on Laskar's orbital solution (eccentricity; Laskar et al., 2011) based on the assumption that a sea level fall must correspond to a major cooling and therefore to a decrease in eccentricity.

Fig. 11: Reconstructed precipitation estimates of the Zambezi catchment from the Oligocene up to Present in the frame of the East Africa: (1) from wells X1 and X3 (see Fig. 1B for location) based on pollen records (this study see text for discussion) and comparison with the reference DSDP Site 231 (Gulf of Aden; Bonnefille, 2010); (2) compilation of the

published precipitation evaluation from scattered outcrops in East Africa mainly based on palaeobotanical data (woods, leaves, pollen grains), (3) regional (Mozambique Channel) and world-scale climatic data. The Mozambique Channel data (unpublished at the moment) were acquired in the frame of the PAMELA Project through a collaboration between geoscientists of Rennes University and palynologists of TOTAL Company (N. Buratti and D. Michoux).

Fig. 12: Summary chart of the stratigraphic data and their possible causes, deformations and climates.

Supplementary materials

Table 1. Interpreted occurrences of planktonic foraminifera in the studied samples from Well X1. The species shown in Figure 8 are written in bold characters. Reworked species from periods older than Campanian are not mentioned.

Table 2. Interpreted occurrences of calcareous nannofossils in the studied samples from Well X1. The species shown in Figure 9 are written in bold characters. Reworked species from periods older than Campanian are not mentioned.

Table 3. Interpreted occurrences of planktonic foraminifera in the studied samples from Well X3. The species shown in Figure 9 are written in bold characters. Reworked species from periods older than Campanian are not mentioned.

Table 4. Interpreted occurrences of calcareous nannofossils in the studied samples from Well X3. The species shown in Figure 9 are written in bold characters. Reworked species from periods older than Campanian are not mentioned.

Table 5. Detailed pollen and spore analyses of the studied samples from Well X1. The abbreviation cf. (confer) is used to specify the most probable taxon after comparison of a fossil pollen with that of several alive taxa; the suffix -type only displays a possible way of pollen identification because the same pollen morphology exists in several other taxa.

Table 6. Detailed pollen and spore analyses of the studied samples from Well X3. Same explanations as for Table 5.

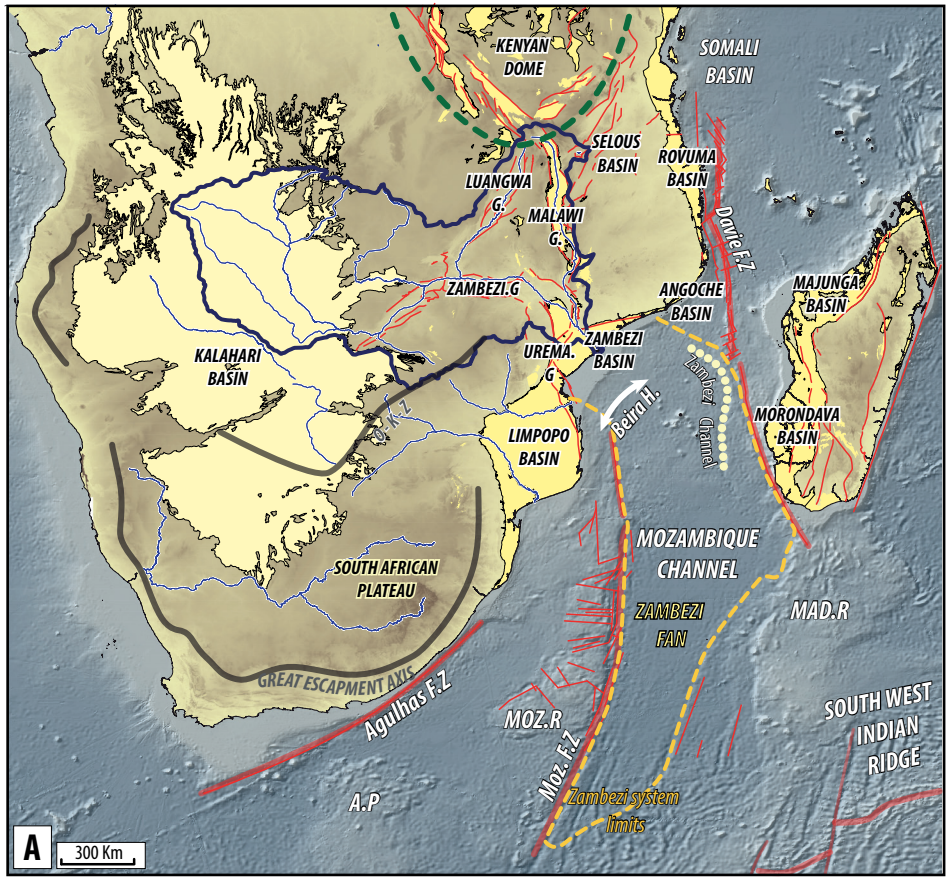

SEDIMENTARY BASINS
- Jurassic to Cenozoic basins
- Kalahari basin

CATCHMENT - DOMES
- Zambezi catchment
- Kenyan dome

FLEXURES - FAULTS
OKZ: Okavango Kalahari Zimbabwe
- Main faults - Fracture zones

OFFSHORE
MAD.R : Madagascar Ridge
MOZ.R : Mozambique Ridge
A.P : Agulhas Plateau

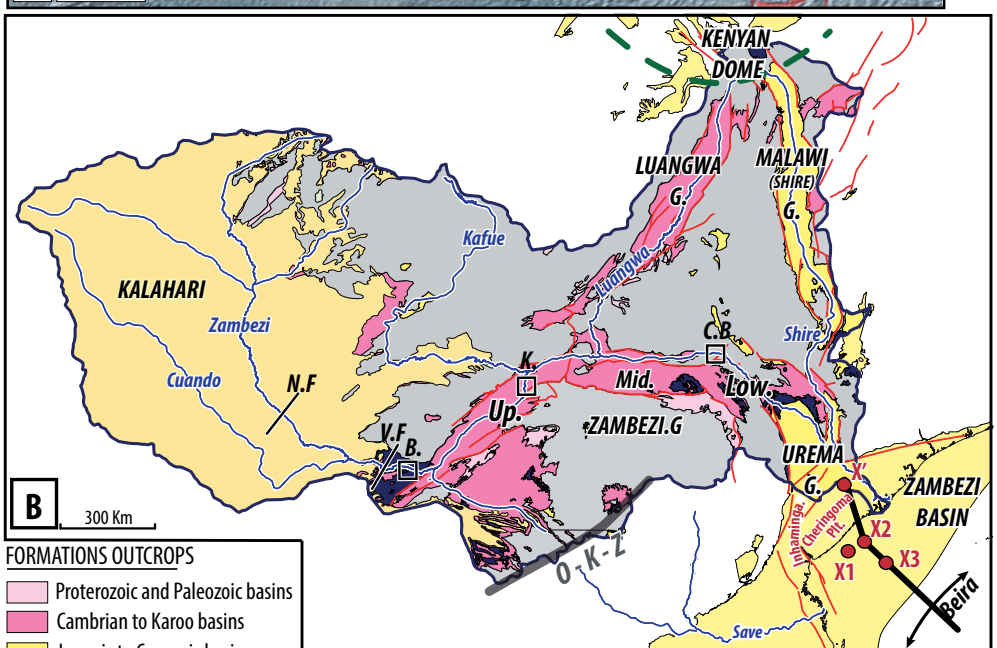

FORMATIONS OUTCROPS
- Proterozoic and Paleozoic basins
- Cambrian to Karoo basins
- Jurassic to Cenozoic basins
- Kalahari Sands
- Basement
- Volcanism

OFFSHORE
- Wells
- Cross section

FLEXURES - FAULTS - DOMES
OKZ: Okavango Kalahari Zimbabwe
- Main faults
- Kenyan dome southern limit

ZAMBEZI FALLS AND GORGES
- Gorges
- Falls

N.F : Ngonye Falls
V.F : Victoria Falls
C.B : Cahora Bassas gorge
K : Kariba gorge
B : Bakota gorge

Figure 1

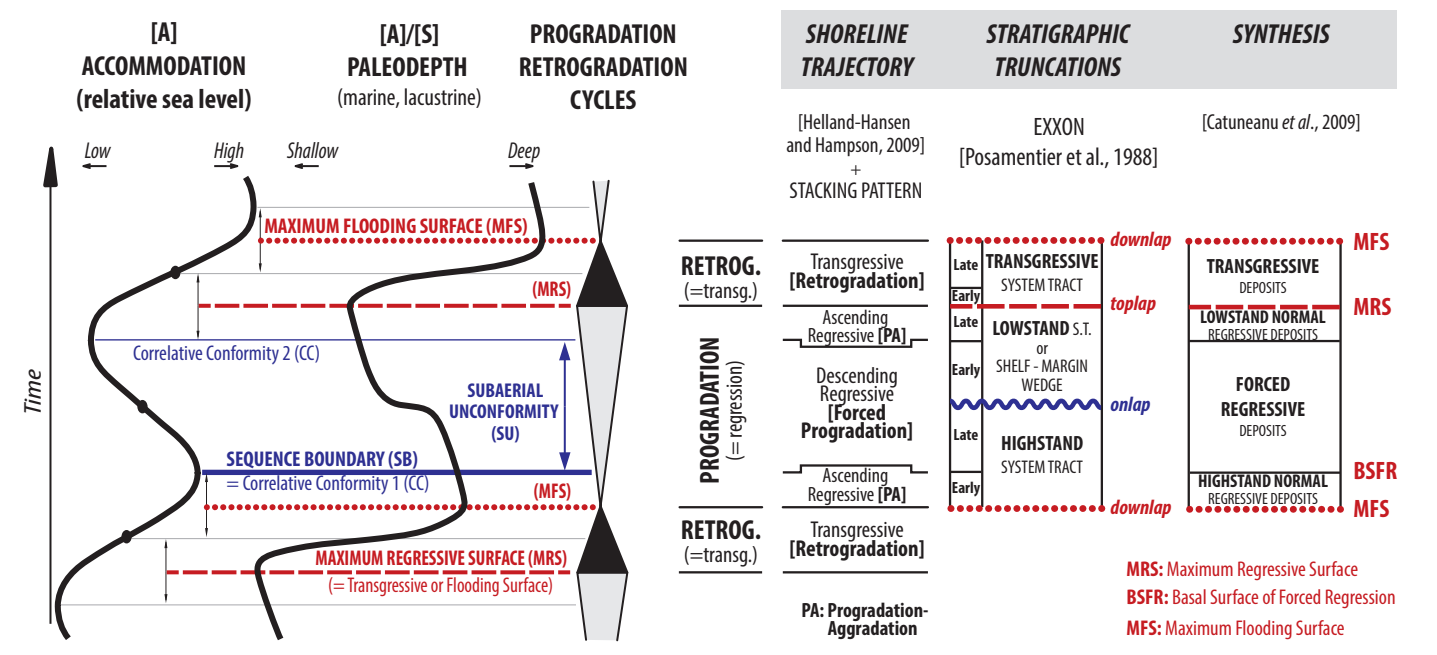
[A]
ACCOMMODATION
(relative sea level)
[A]/[S]
PALEODEPTH
(marine, lacustrine)
PROGRADATION
RETROGRADATION
CYCLES
Low
High
Shallow
Deep
Time
MAXIMUM FLOODING SURFACE (MFS)
(MRS)
Correlative Conformity 2 (CC)
SUBAERIAL
UNCONFORMITY
(SU)
SEQUENCE BOUNDARY (SB)
= Correlative Conformity 1 (CC)
(MFS)
MAXIMUM REGRESSIVE SURFACE (MRS)
(= Transgressive or Flooding Surface)
SHORELINE
TRAJECTORY
STRATIGRAPHIC
TRUNCATIONS
SYNTHESIS
[Helland-Hansen
and Hampson, 2009]
+
STACKING PATTERN
EXXON
[Posamentier et al., 1988]
[Catuneanu et al., 2009]
RETROG.
(=transg.)
PROGRADATION
(= regression)
RETROG.
(=transg.)
Transgressive
[Retrogradation]
Ascending
Regressive [PA]
Descending
Regressive
[Forced
Progradation]
Ascending
Regressive [PA]
Transgressive
[Retrogradation]
PA: Progradation-
Aggradation
Late
Early
Late
Early
Late
Early
TRANSGRESSIVE
SYSTEM TRACT
LOWSTAND S.T.
or
SHELF - MARGIN
WEDGE
HIGHSTAND
SYSTEM TRACT
downlap
toplap
onlap
downlap
TRANSGRESSIVE
DEPOSITS
LOWSTAND NORMAL
REGRESSIVE DEPOSITS
FORCED
REGRESSIVE
DEPOSITS
HIGHSTAND NORMAL
REGRESSIVE DEPOSITS
MFS
MRS
BSFR
MFS
MRS: Maximum Regressive Surface
BSFR: Basal Surface of Forced Regression
MFS: Maximum Flooding Surface

Figure 2

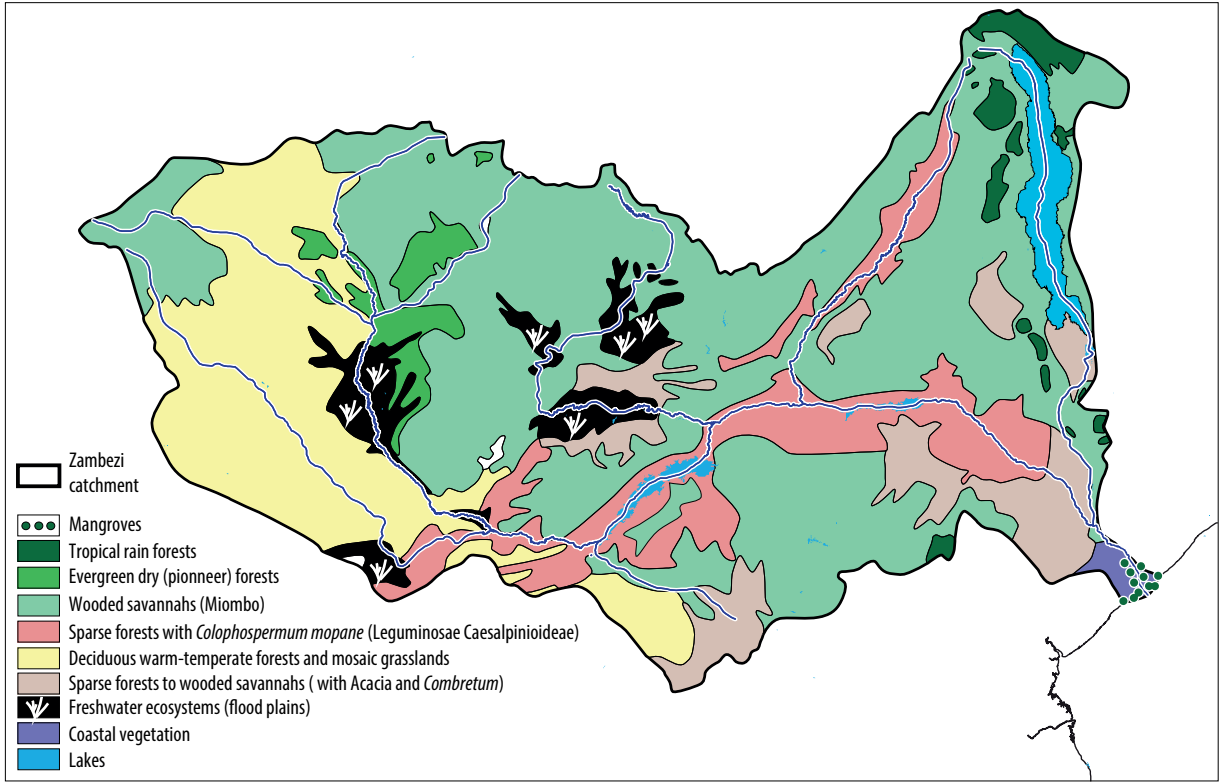
Zambezi catchment
Mangroves
Tropical rain forests
Evergreen dry (pionneer) forests
Wooded savannahs (Miombo)
Sparse forests with *Colophospermum mopane* (Leguminosae Caesalpinioideae)
Deciduous warm-temperate forests and mosaic grasslands
Sparse forests to wooded savannahs (with Acacia and *Combretum*)
Freshwater ecosystems (flood plains)
Coastal vegetation
Lakes

Figure 3

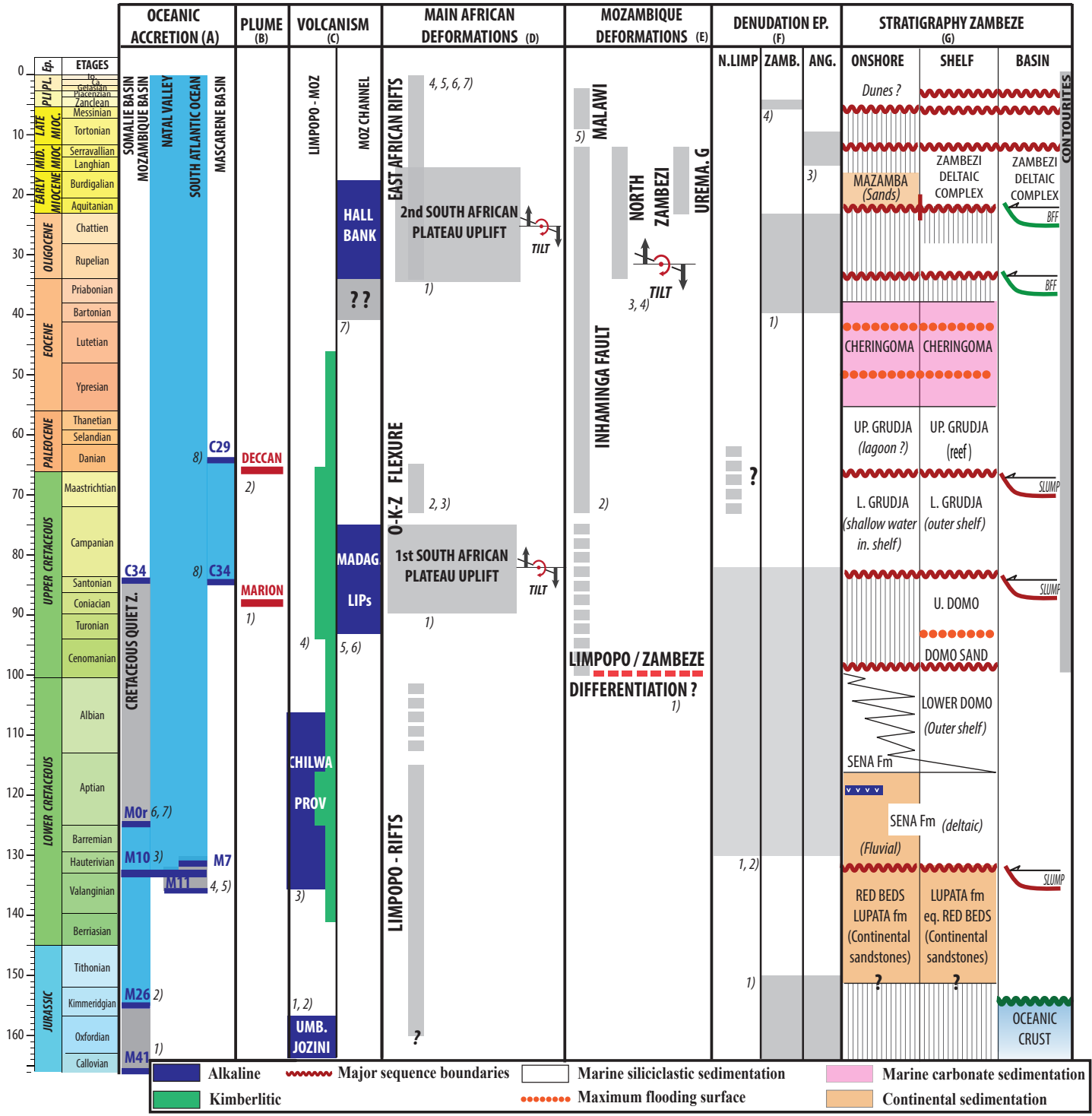

Compilation of data from literature :

A) *: (1) Leinweber et al., 2013; (2) Konig and Jokat, 2010; 3) Goodlad et al., 1982; (4) Leinweber and Jokat, 2011; (5) Tikku et al., 2002; (6) Cochran, 1988; (7) Raillard,1990 ; (8) Plummer and Belle, 1995.*

B)*: (1) Storey et al., 1995; (2)Mahoney et al., 2002.*

C) *: (1) Salman and Abdula, 1995; (2) Pekkala, 2008; (3) Wooley, 1987; (4) Jelsma et al., 2004; (5) Raillard, 1990; (6) Bardintzeff et al., 2010; (7) Courgeon et al., 2016.*

D) *: (1) Baby, 2017; (2) Moore, 1999; (3) Du Toit, 1933; (4) Ebinger 1989; (5) Chorowicz, 2005; (6) Macgregor, 2015; (7) Simon et al., 2017*

E) *: (1) Nairn et al., (1991), (2) Flores, 1973; (3) Lafourcade, 1984; (4) Baby, 2017; (5) Ebinger,1989, 1993.*

F)*: (1) Daszinnies, 2006; (2) Belton and Raab, 2010; (3) Mortimer, 2006; (4) Fernandes et al., 2015.*

G)*: (1) Flores, 1973; (2) Virlogeux, 1987; (3) Nairn et al., 1991; (4) Salman and Abdula, 1995.*

Figure 4

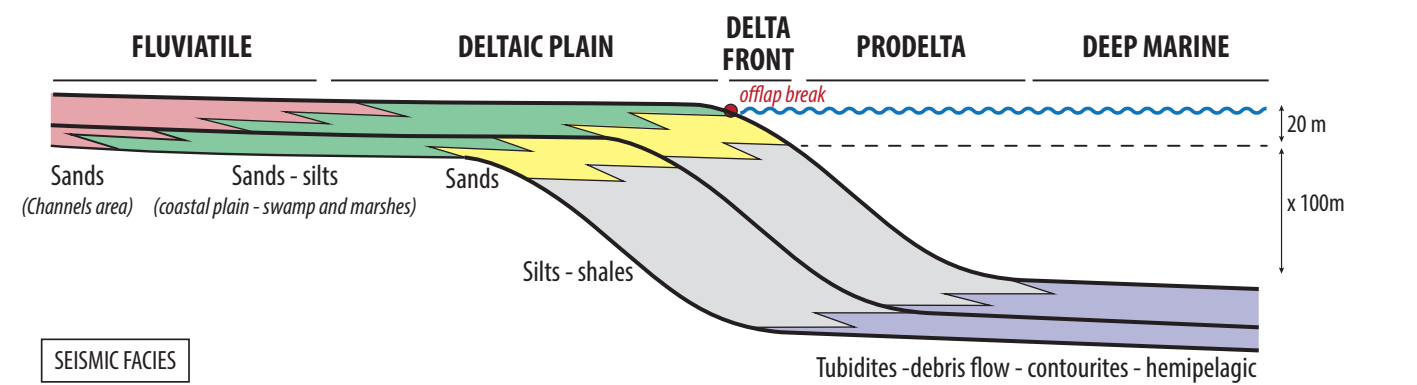

SEISMIC FACIES

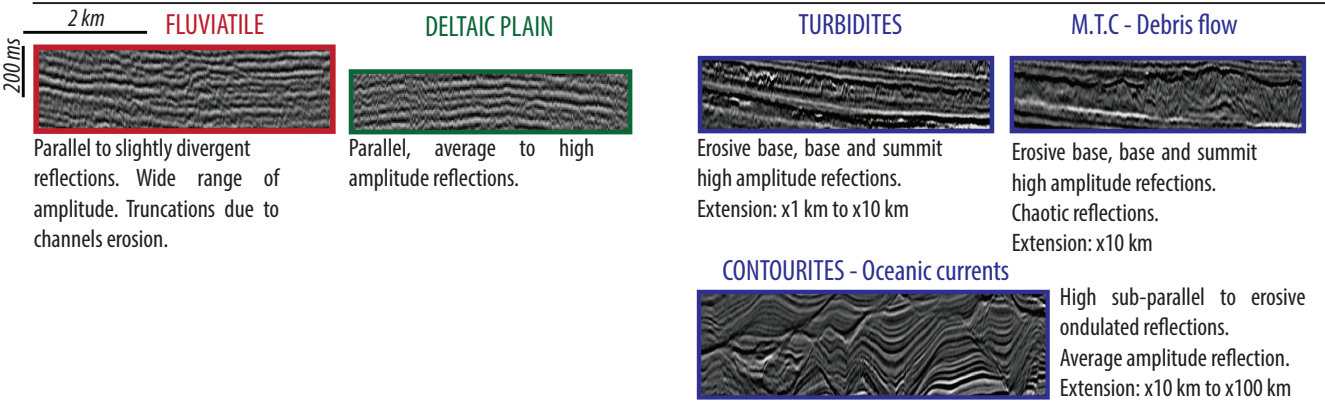

Parallel to slightly divergent reflections. Wide range of amplitude. Truncations due to channels erosion.

Parallel, average to high amplitude reflections.

Erosive base, base and summit high amplitude refections.
Extension: x1 km to x10 km

Erosive base, base and summit high amplitude refections.
Chaotic reflections.
Extension: x10 km

High sub-parallel to erosive ondulated reflections.
Average amplitude reflection.
Extension: x10 km to x100 km

Figure 5

AGE MODEL

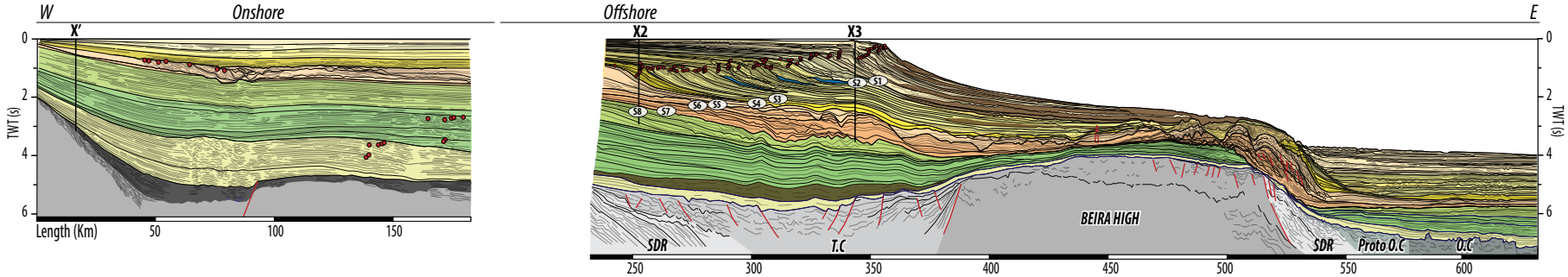

SEDIMENTARY DEPOSITS

- PLEISTOCENE (2.8 - 0 My)
- PLIOCENE (5.6 - 2.8 My)
- LATE MIOCENE (11.6 - 5.6 My)
- EARLY - MiDDLE MIOCENE (26 - 11.6 My)
- OLIGOCENE (36.2 - 26 My)
- EOCENE (55.8- 33.9 My)
- PALEOCENE (66 - 55.8 My)
- LATE CRETACEOUS (100.5 - 66 My)
- EARLY CRETACEOUS (130 - 100.5 My)
- EARLY CRETACEOUS (145? - 130 My)
- Slope apron
- Slump / Debris flow

BASEMENT NATURE

- SDR — Seaward Dipping Reflectors
- T.C — Transitionnal Crust
- Proto O.C — Proto Oceanic Crust
- O.C — Oceanic Crust
- C.C — Continental Crust
- Karoo Volcanics

SHORELINE TRAJECTORY

- Offlap break

SEDIMENTARY ENVIRONMENTS

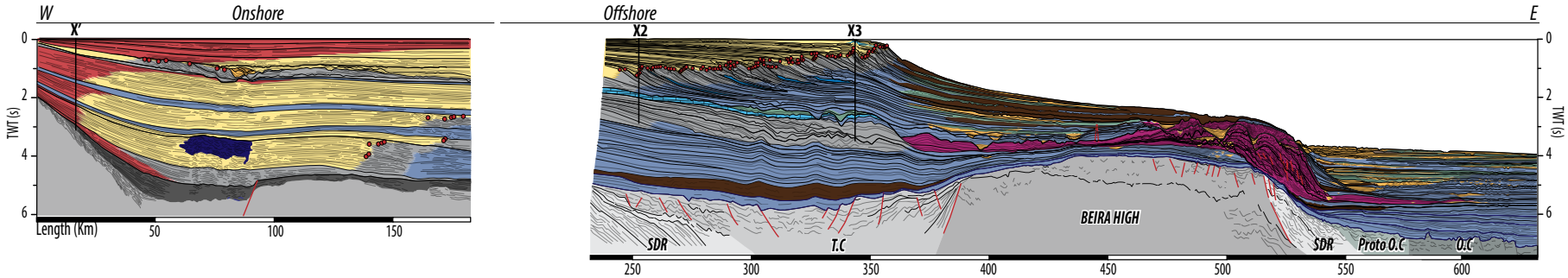

SEDIMENTARY DEPOSITS

- Fluvial deposits
- Coastal sands
  Littoral deposits
- Delta front to Pro delta: slope
  Upper offshore: silts to fine sands
- Silty, shaly deep sea turbiditic deposits / levee deposits
- Sandy turbiditic lobe
  Inner channel deposits
- Hemipelagite shale / silts
- Contouritic deposits
- Karoo volcanics
- Volcanism
- Carbonates
- Slump / debris flow

BASEMENT NATURE

- SDR — Seaward Dipping Reflectors
- T.C — Transitionnal Crust
- C.C — Continental Crust
- Proto O.C — Proto Oceanic Crust
- O.C: Oceanic Crust

SHORELINE TRAJECTORY

- Offlap break

Figure 6

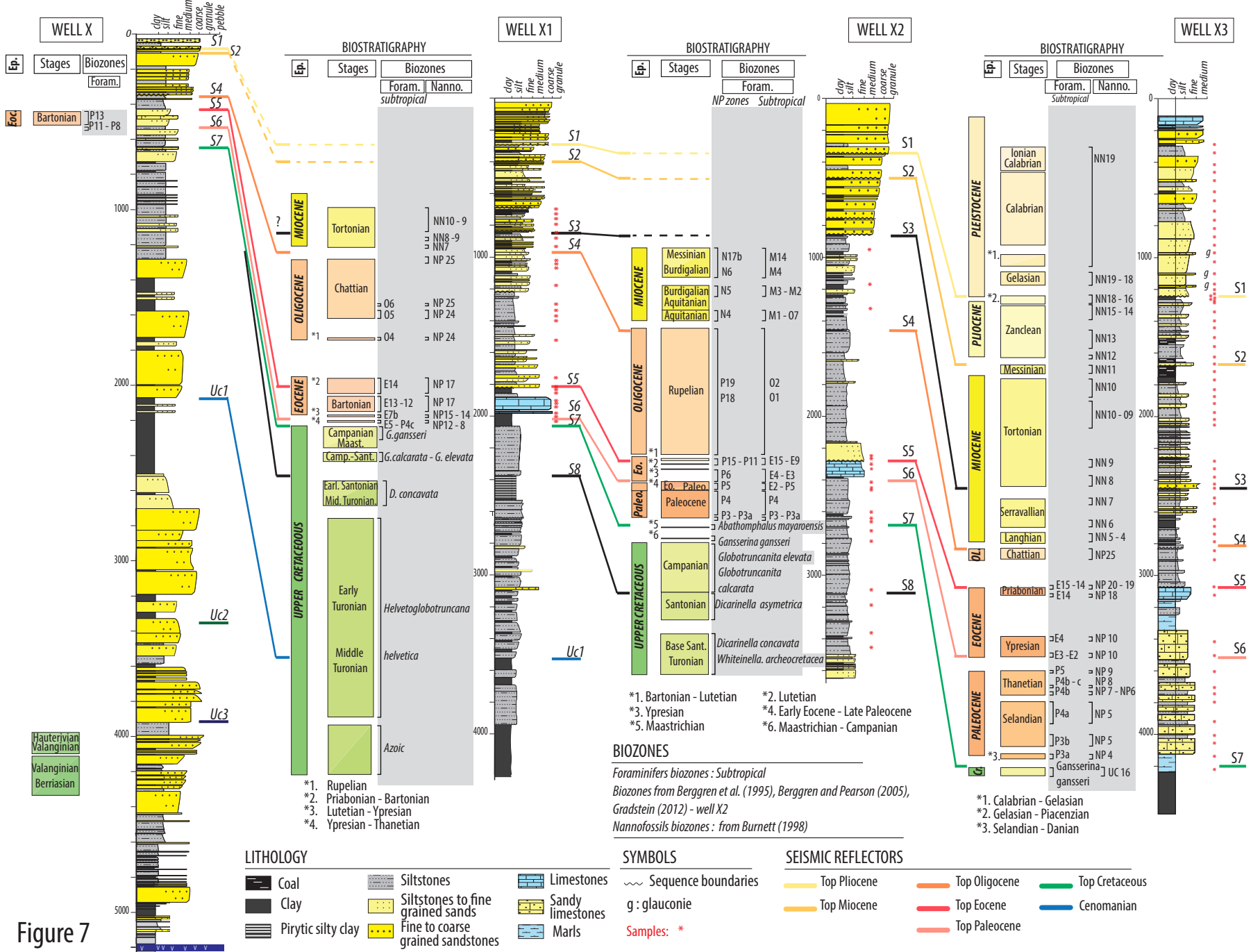
WELL X
WELL X1
WELL X2
WELL X3
BIOSTRATIGRAPHY
Ep.
Stages
Biozones
Foram.
Nanno.
subtropical
NP zones
Bartonian
P13
P11 - P8
MIOCENE
OLIGOCENE
EOCENE
UPPER CRETACEOUS
Tortonian
Chattian
Campanian Maast.
Camp.-Sant.
Earl. Santonian Mid. Turonian.
Early Turonian
Middle Turonian
Helvetoglobotruncana
helvetica
Azoic
G.gansseri
G.calcarata - G. elevata
D. concavata
NN10 - 9
NN8 -9
NN7
NP 25
NP 24
NP 17
NP15 - 14
NP12 - 8
E14
E13 -12
E7b
E5 - P4c
O6
O5
O4
Messinian
Burdigalian
Aquitanian
Rupelian
Paleocene
Eo.
Paleo.
Santonian
Base Sant. Turonian
N17b
N6
N5
N4
P19
P18
P4
P3 - P3a
P15 - P11
P6
P5
M14
M4
M3 - M2
M1 - 07
02
01
E15 - E9
E4 - E3
E2 - P5
Abathomphalus mayaroensis
Gansserina gansseri
Globotruncanita elevata
Globotruncanita calcarata
Dicarinella asymetrica
Dicarinella concavata
Whiteinella. archeocretacea
PLEISTOCENE
PLIOCENE
MIOCENE
OLIGOCENE
EOCENE
PALEOCENE
Ionian
Calabrian
Gelasian
Zanclean
Messinian
Tortonian
Serravallian
Langhian
Chattian
Priabonian
Ypresian
Thanetian
Selandian
Gansserina gansseri
NN19
NN19 - 18
NN18 - 16
NN15 - 14
NN13
NN12
NN11
NN10
NN10 - 09
NN 9
NN 8
NN 7
NN 6
NN 5 - 4
NP25
E15 -14
E14
NP 20 - 19
NP 18
E4
E3 -E2
NP 10
P5
P4b - c
P4b
NP 9
NP 8
NP 7 - NP6
P4a
NP 5
P3b
P3a
NP 4
UC 16
Hauterivian Valanginian
Valanginian Berriasian
S1
S2
S3
S4
S5
S6
S7
S8
Uc1
Uc2
Uc3
*1. Bartonian - Lutetian
*2. Lutetian
*3. Ypresian
*4. Early Eocene - Late Paleocene
*5. Maastrichian
*6. Maastrichian - Campanian
*1. Rupelian
*2. Priabonian - Bartonian
*3. Lutetian - Ypresian
*4. Ypresian - Thanetian
*1. Calabrian - Gelasian
*2. Gelasian - Piacenzian
*3. Selandian - Danian
BIOZONES
Foraminifers biozones : Subtropical
Biozones from Berggren et al. (1995), Berggren and Pearson (2005), Gradstein (2012) - well X2
Nannofossils biozones : from Burnett (1998)
LITHOLOGY
Coal
Clay
Pirytic silty clay
Siltstones
Siltstones to fine grained sands
Fine to coarse grained sandstones
Limestones
Sandy limestones
Marls
SYMBOLS
Sequence boundaries
g : glauconie
Samples: *
SEISMIC REFLECTORS
Top Pliocene
Top Miocene
Top Oligocene
Top Eocene
Top Paleocene
Top Cretaceous
Cenomanian

Figure 7

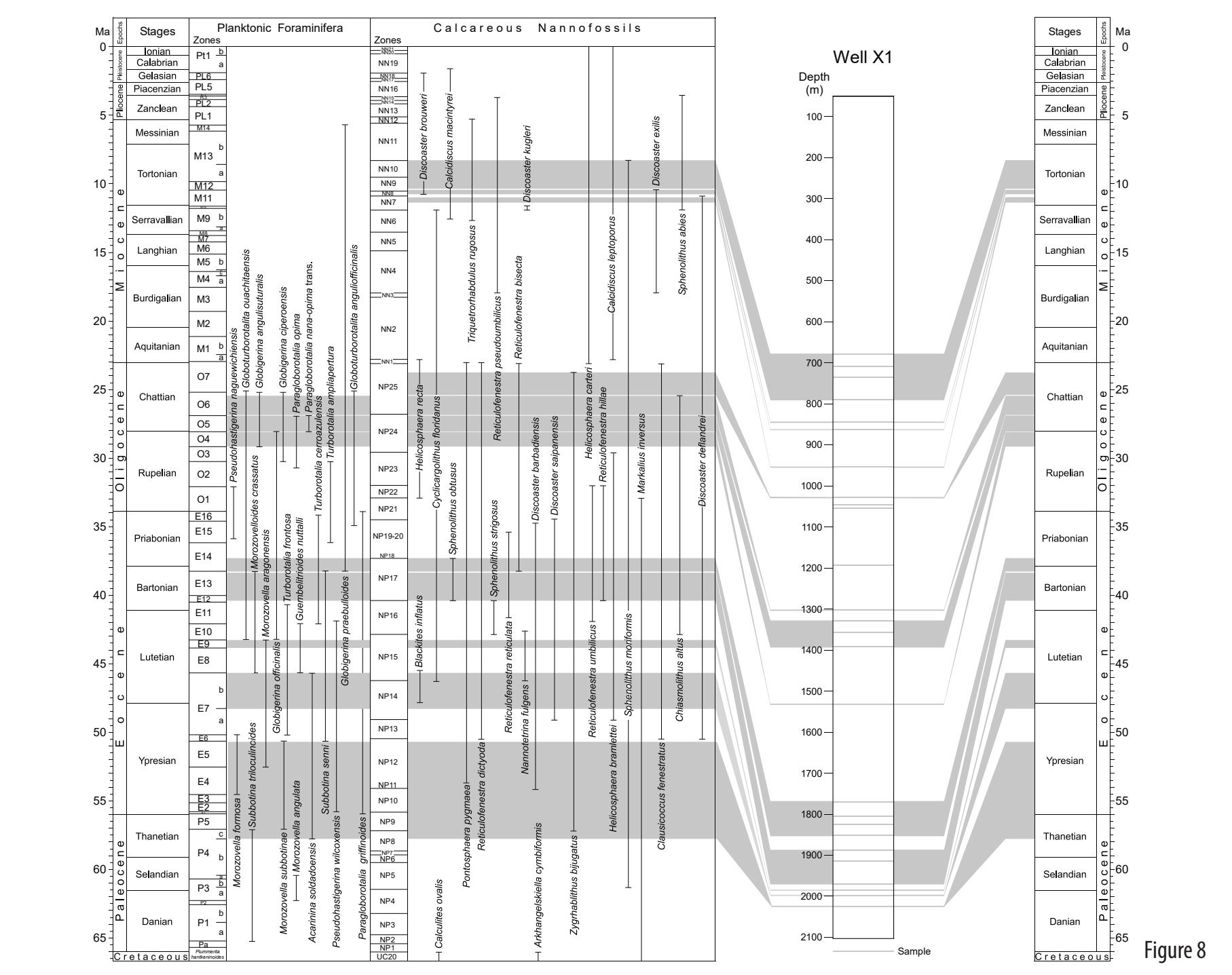
Ma
Stages
Epochs
Planktonic Foraminifera
Zones
Calcareous Nannofossils
Zones
Ionian
Calabrian
Gelasian
Piacenzian
Zanclean
Messinian
Tortonian
Serravallian
Langhian
Burdigalian
Aquitanian
Chattian
Rupelian
Priabonian
Bartonian
Lutetian
Ypresian
Thanetian
Selandian
Danian
Cretaceous
Pleistocene
Pliocene
Miocene
Oligocene
Eocene
Paleocene
Pt1
PL6
PL5
PL2
PL1
M14
M13
M12
M11
M9
M7
M6
M5
M4
M3
M2
M1
O7
O6
O5
O4
O3
O2
O1
E16
E15
E14
E13
E12
E11
E10
E9
E8
E7
E6
E5
E4
E3
E2
P5
P4
P3
P2
P1
Pa
Plummerita hantkeninoides
NN19
NN18
NN17
NN16
NN15
NN14
NN13
NN12
NN11
NN10
NN9
NN8
NN7
NN6
NN5
NN4
NN3
NN2
NN1
NP25
NP24
NP23
NP22
NP21
NP19-20
NP18
NP17
NP16
NP15
NP14
NP13
NP12
NP11
NP10
NP9
NP8
NP7
NP6
NP5
NP4
NP3
NP2
NP1
UC20
Pseudohastigerina naguewichiensis
Globoturborotalita ouachitaensis
Morozovelloides crassatus
Morozovella aragonensis
Globigerina angulisuturalis
Globigerina officinalis
Turborotalia frontosa
Guembelitroides nuttalli
Globigerina ciperoensis
Paragloborotalia opima
Paragloborotalia nana-opima trans.
Turborotalia cerroazulensis
Turborotalia ampliapertura
Globoturborotalita anguliofficinalis
Globigerina praebulloides
Morozovella formosa
Subbotina trilociulinicides
Morozovella subbotinae
Morozovella angulata
Acarinina soldadoensis
Subbotina senni
Pseudohastigerina wilcoxensis
Paragloborotalia griffinoides
Discoaster brouweri
Calcidiscus macintyrei
Triquetrorhabdulus rugosus
Reticulofenestra pseudoumbilicus
Reticulofenestra bisecta
Discoaster kugleri
Discoaster barbadiensis
Discoaster saipanensis
Helicosphaera recta
Cyclicargolithus floridanus
Sphenolithus obtusus
Blackites inflatus
Sphenolithus strigosus
Reticulofenestra reticulata
Nannotetrina fulgens
Arkhangelskiella cymbiformis
Pontosphaera pygmaea
Reticulofenestra dictyoda
Calculites ovalis
Zygrhablithus bijugatus
Helicosphaera carteri
Reticulofenestra umbilicus
Reticulofenestra hillae
Helicosphaera bramlettei
Sphenolithus moniformis
Markalius inversus
Clausicoccus fenestratus
Calcidiscus leptoporus
Discoaster exilis
Chiasmolithus altus
Sphenolithus abies
Discoaster deflandrei
Well X1
Depth
(m)
100
200
300
400
500
600
700
800
900
1000
1100
1200
1300
1400
1500
1600
1700
1800
1900
2000
2100
Sample

Figure 8

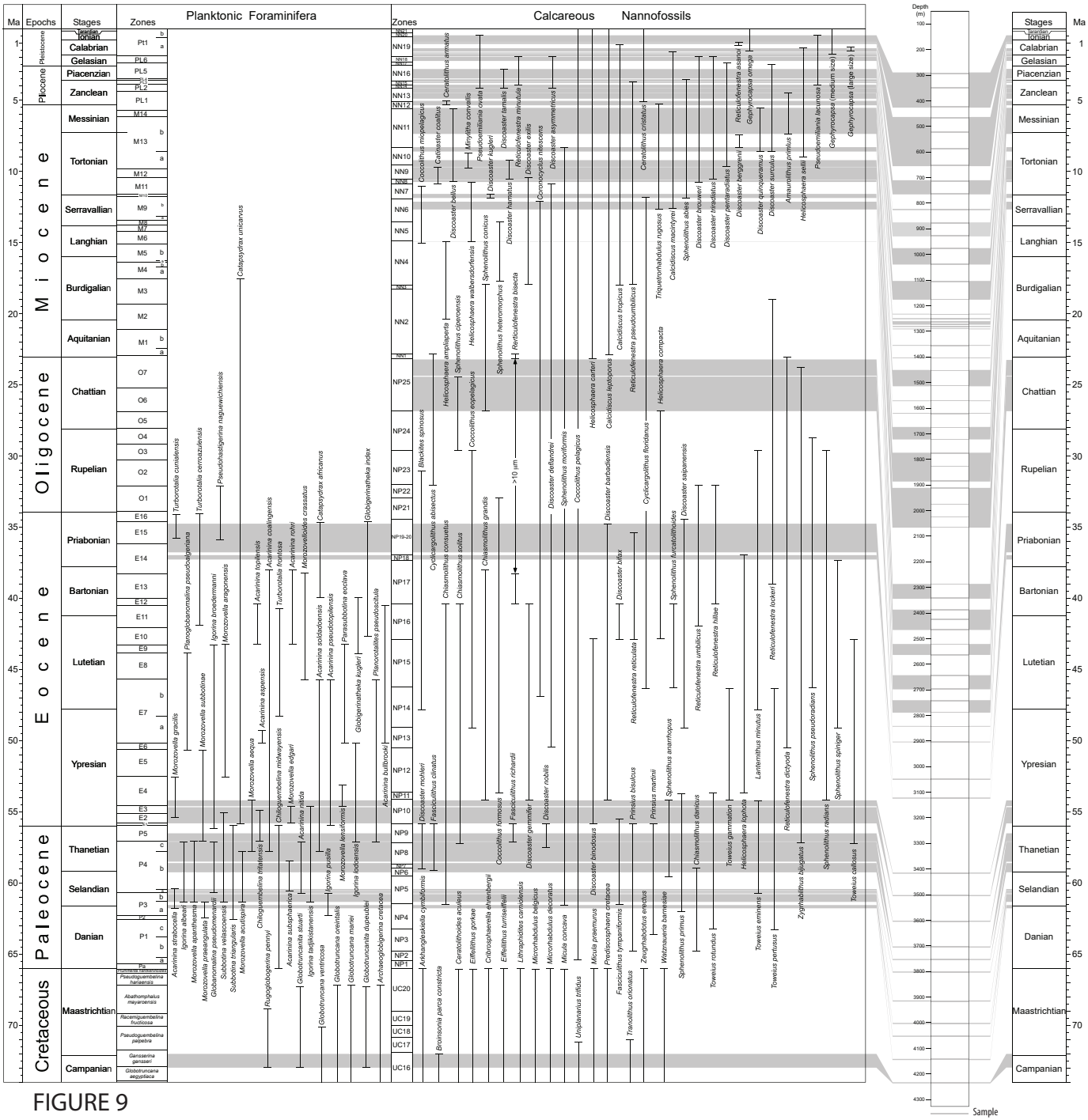
Well X3
Planktonic Foraminifera
Calcareous Nannofossils
Ma
Epochs
Stages
Zones
Depth (m)
Sample
Cretaceous
Paleocene
Eocene
Oligocene
Miocene
Pliocene
Pleistocene
Ionian
Calabrian
Gelasian
Piacenzian
Zanclean
Messinian
Tortonian
Serravallian
Langhian
Burdigalian
Aquitanian
Chattian
Rupelian
Priabonian
Bartonian
Lutetian
Ypresian
Thanetian
Selandian
Danian
Maastrichtian
Campanian

FIGURE 9

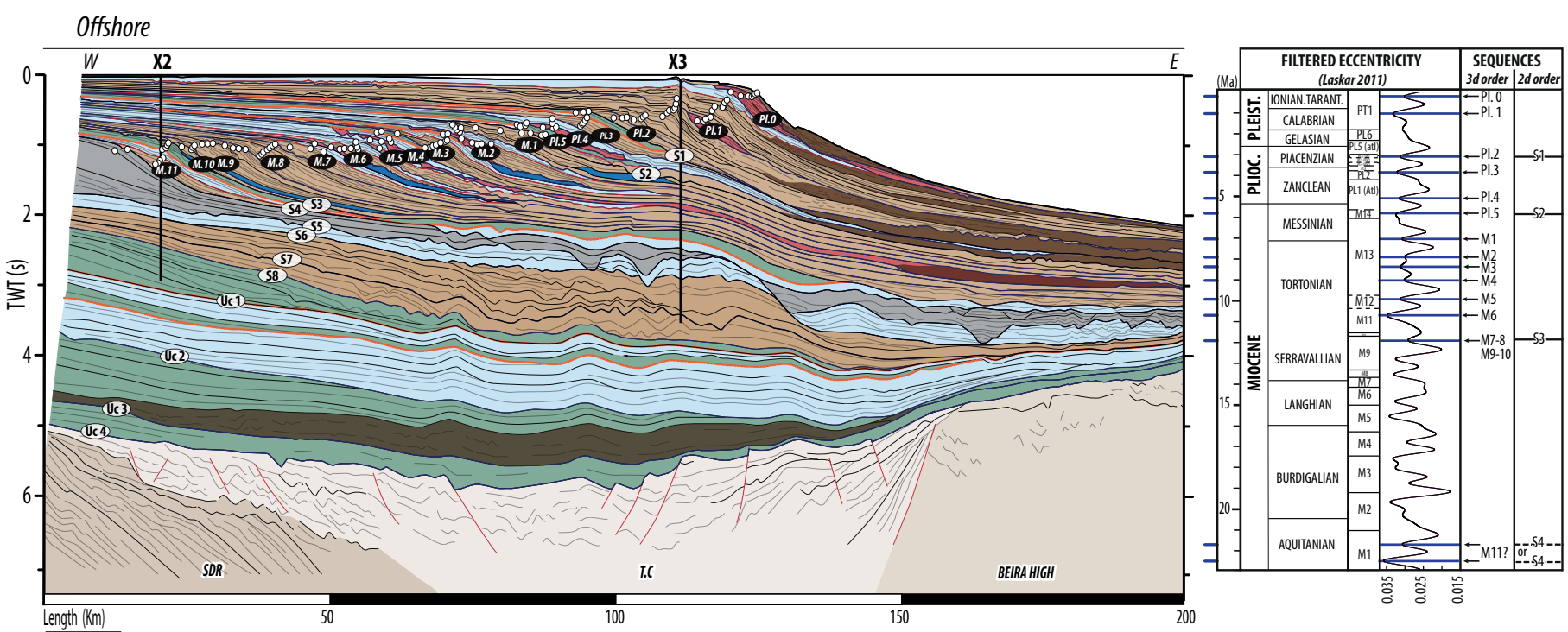
Offshore
W
X2
X3
E
TWT (s)
0
2
4
6
M.11
M.10
M.9
M.8
M.7
M.6
M.5
M.4
M.3
M.2
M.1
Pl.5
Pl.4
Pl.3
Pl.2
Pl.1
Pl.0
S1
S2
S3
S4
S5
S6
S7
S8
Uc 1
Uc 2
Uc 3
Uc 4
SDR
T.C
BEIRA HIGH
Length (Km)
50
100
150
200
(Ma)
FILTERED ECCENTRICITY
(Laskar 2011)
SEQUENCES
3d order
2d order
PLEIST.
PLIOC.
MIOCENE
IONIAN.TARANT.
CALABRIAN
GELASIAN
PIACENZIAN
ZANCLEAN
MESSINIAN
TORTONIAN
SERRAVALLIAN
LANGHIAN
BURDIGALIAN
AQUITANIAN
PT1
PL6
PL5 (atl)
PL4
PL3
PL2
PL1 (Atl)
M14
M13
M12
M11
M9
M8
M7
M6
M5
M4
M3
M2
M1
5
10
15
20
Pl. 0
Pl. 1
Pl.2
Pl.3
Pl.4
Pl.5
M1
M2
M3
M4
M5
M6
M7-8
M9-10
M11?
S1
S2
S3
S4
or
S4
0.035
0.025
0.015
SYSTEMS TRACKS
TRANSGRESSIVE
HIGHSTAND
LOWSTAND
MRS (Maximum Regressive Surface)
SB (Sequence Boundary)
FALLING STAGE
UNDETERMINED
MFS (Maximum Flooding Surface)
OTHERS
Offlap break
SLOPE APRON
SLUMPS / DEBRIS FLOW
BASEMENT NATURE
SDR
Seaward Dipping Reflectors
T.C
Transitionnal Crust
Beira High
Continental Crust
SEQUENCES
Third order sequences (Laskar, 2011)
Second order sequences (50 - 3 My)

Figure 10

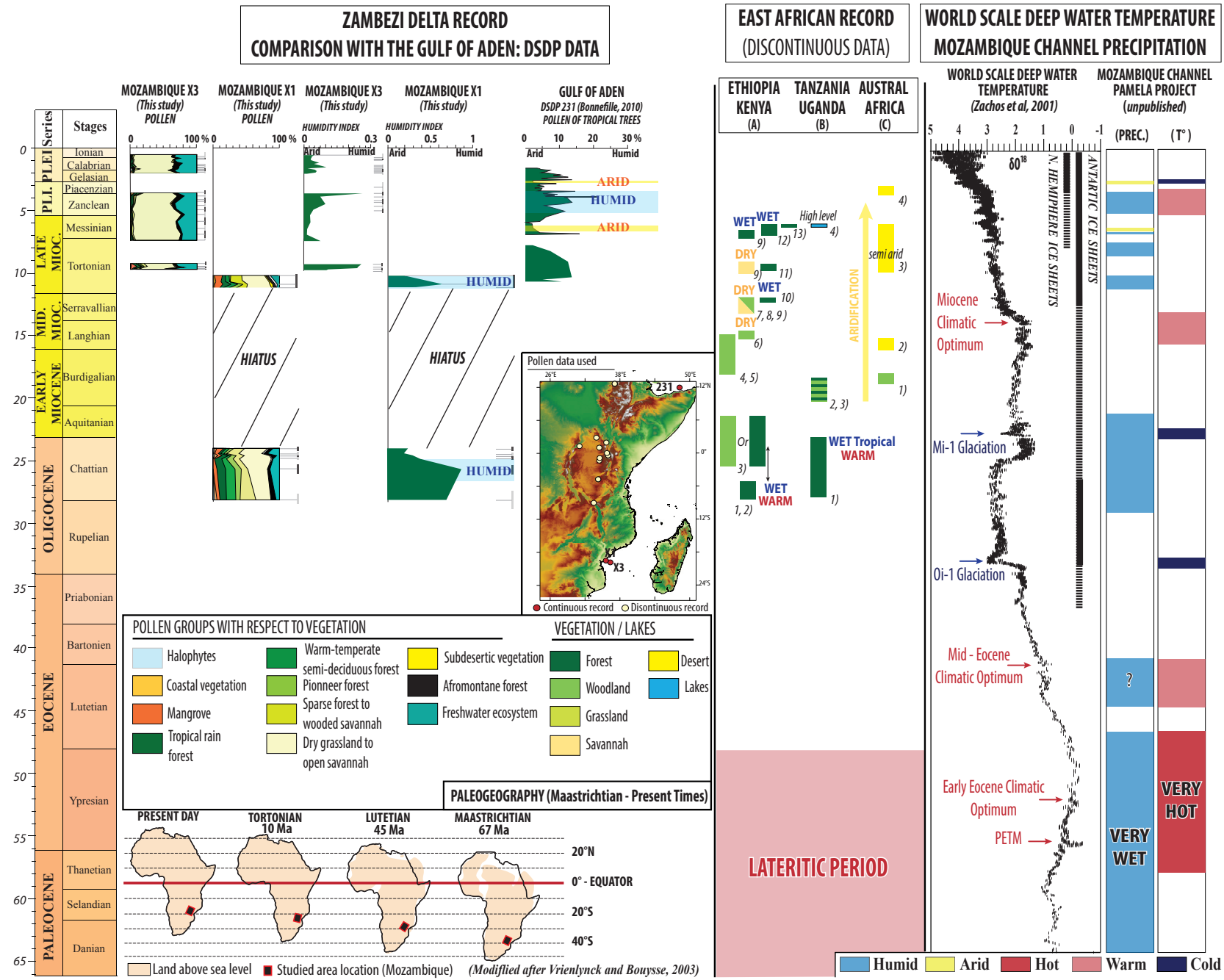

Compilation of data from literature *: **A)** : (1) Pan et al., 2006; (2) Jacobs et al., 2005, (3) Vincens et al., 2006 (4) Bestland and Retallack, 1993; (5) Collinson et al., 2009; (6) Retallack, 2002; (7) Rasmussen et al., (2017); (8) Jacobs and Deino, 1996; (9) Jacobs, 2002; (10) Jacobs and Kabuye, 1987; (11) Sakai et al., 2010; (12) Kingston et al., 2002; (13) De Franceschi et al., 2016. **(B):** (1) Damblon et al., 1998; (2) Pickford, 2002; (3) Pickford, 2004; (4) Simon et al., 2017. **(C):** (1) Neumann and Bamford, 2015; (2) Pickford, 2014; (3) Dupont et al., 2011; (4) Hoetzel et al., 2017.*

Figure 11

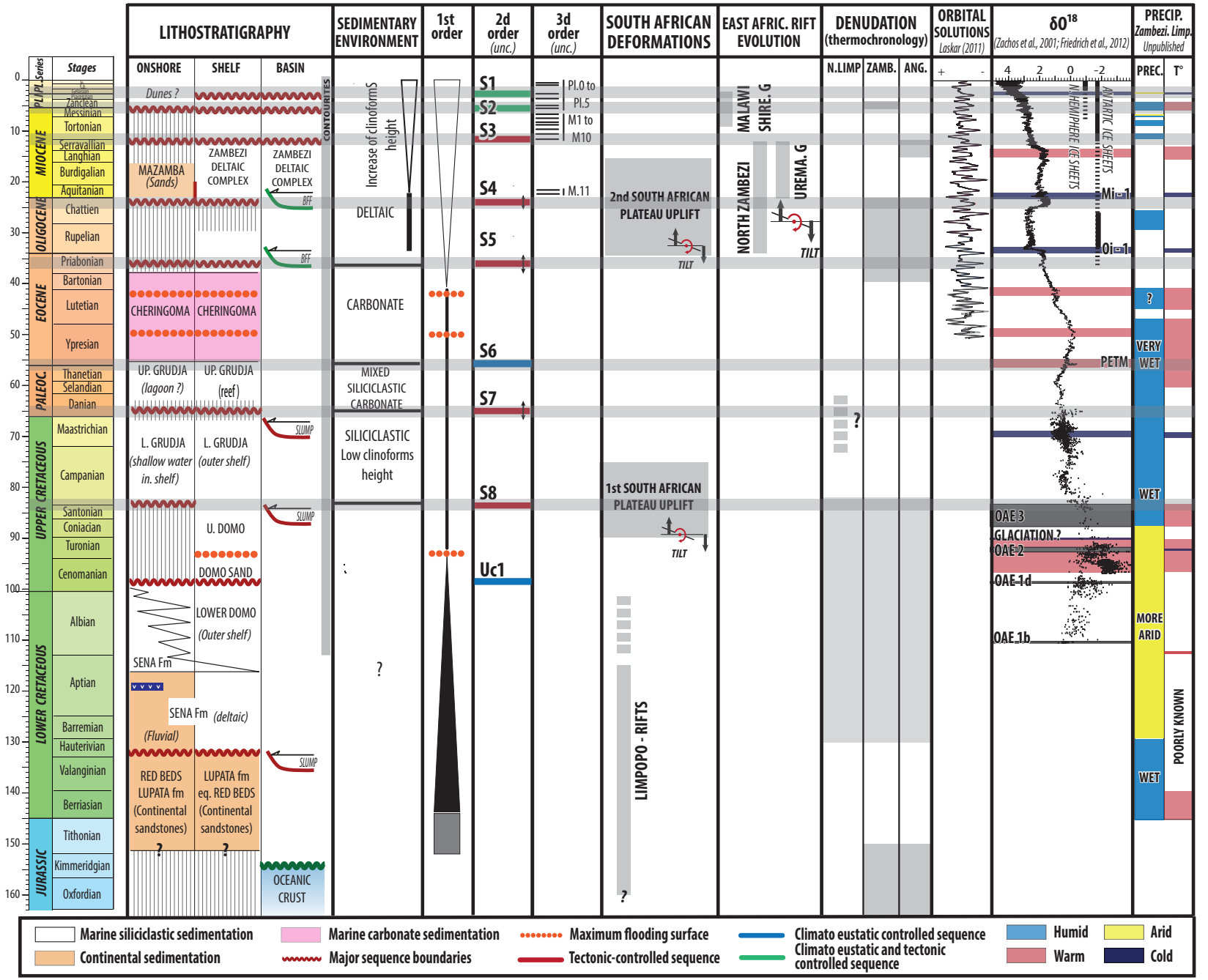
LITHOSTRATIGRAPHY
ONSHORE
SHELF
BASIN
SEDIMENTARY ENVIRONMENT
1st order
2d order (unc.)
3d order (unc.)
SOUTH AFRICAN DEFORMATIONS
EAST AFRIC. RIFT EVOLUTION
DENUDATION (thermochronology)
N.LIMP
ZAMB.
ANG.
ORBITAL SOLUTIONS Laskar (2011)
δO18 (Zachos et al., 2001; Friedrich et al., 2012)
PRECIP. Zambezi. Limp. Unpublished
PREC.
T°
Series
Stages
PLIOCENE
MIOCENE
OLIGOCENE
EOCENE
PALEOC.
UPPER CRETACEOUS
LOWER CRETACEOUS
JURASSIC
Dunes ?
MAZAMBA (Sands)
ZAMBEZI DELTAIC COMPLEX
CONTOURITES
BFF
CHERINGOMA
UP. GRUDJA (lagoon ?)
UP. GRUDJA (reef)
L. GRUDJA (shallow water in. shelf)
L. GRUDJA (outer shelf)
U. DOMO
DOMO SAND
LOWER DOMO (Outer shelf)
SENA Fm
SENA Fm (deltaic)
(Fluvial)
RED BEDS LUPATA fm (Continental sandstones)
LUPATA fm eq. RED BEDS (Continental sandstones)
SLUMP
OCEANIC CRUST
Increase of clinoforms height
DELTAIC
CARBONATE
MIXED SILICICLASTIC CARBONATE
SILICICLASTIC Low clinoforms height
S1
S2
S3
S4
S5
S6
S7
S8
Uc1
Pl.0 to Pl.5
M1 to M10
M.11
2nd SOUTH AFRICAN PLATEAU UPLIFT
1st SOUTH AFRICAN PLATEAU UPLIFT
TILT
LIMPOPO - RIFTS
MALAWI
SHIRE. G
NORTH ZAMBEZI
UREMA. G
N.HEMISPHERE ICE SHEETS
ANTARCTIC ICE SHEETS
Mi-1
Oi-1
PETM
OAE 3
GLACIATION ?
OAE 2
OAE 1d
OAE 1b
VERY WET
WET
MORE ARID
POORLY KNOWN
Marine siliciclastic sedimentation
Continental sedimentation
Marine carbonate sedimentation
Major sequence boundaries
Maximum flooding surface
Tectonic-controlled sequence
Climato eustatic controlled sequence
Climato eustatic and tectonic controlled sequence
Humid
Warm
Arid
Cold

Figure 12

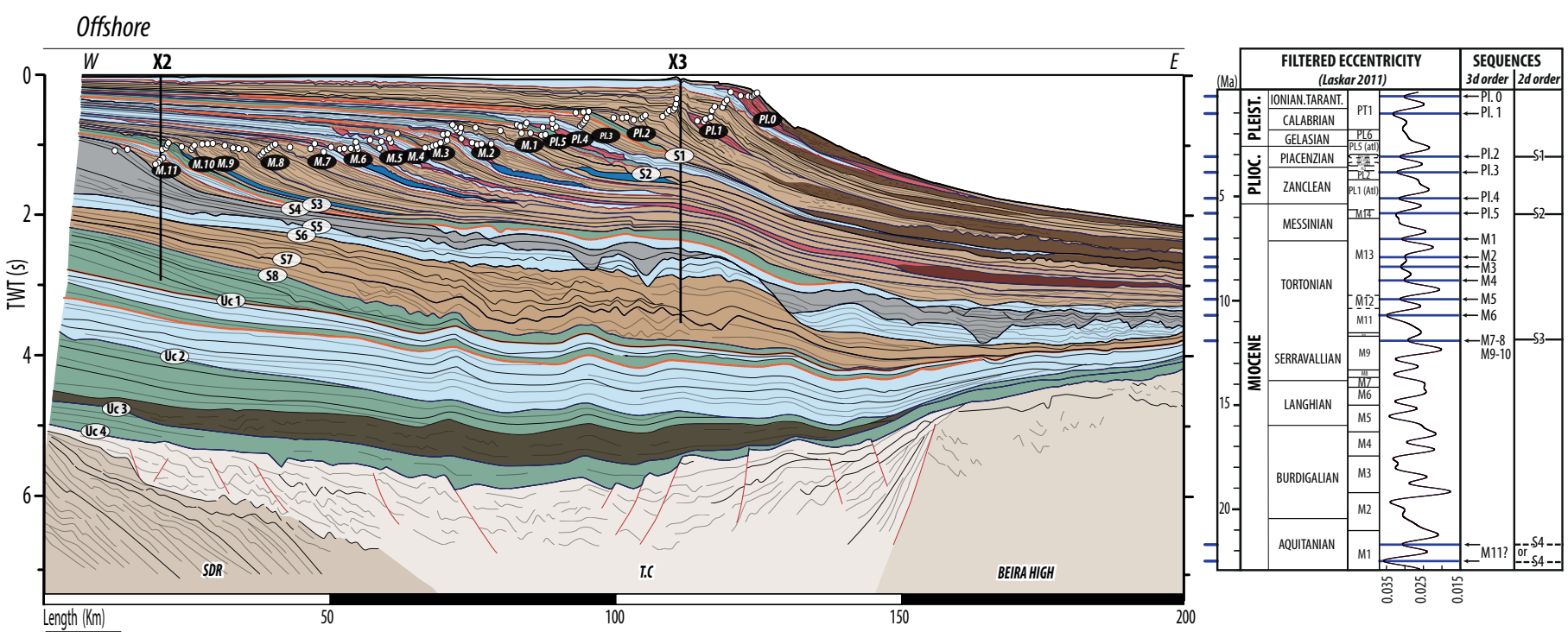
Offshore
W
X2
X3
E
TWT (s)
0
2
4
6
M.11
M.10
M.9
M.8
M.7
M.6
M.5
M.4
M.3
M.2
M.1
Pl.5
Pl.4
Pl.3
Pl.2
Pl.1
Pl.0
S1
S2
S3
S4
S5
S6
S7
S8
Uc 1
Uc 2
Uc 3
Uc 4
SDR
T.C
BEIRA HIGH
Length (Km)
50
100
150
200
(Ma)
FILTERED ECCENTRICITY
(Laskar 2011)
SEQUENCES
3d order
2d order
PLEIST.
PLIOC.
MIOCENE
IONIAN.TARANT.
CALABRIAN
GELASIAN
PIACENZIAN
ZANCLEAN
MESSINIAN
TORTONIAN
SERRAVALLIAN
LANGHIAN
BURDIGALIAN
AQUITANIAN
PT1
PL6
PL5 (atl)
PL4
PL3
PL2
PL1 (Atl)
M14
M13
M12
M11
M9
M8
M7
M6
M5
M4
M3
M2
M1
5
10
15
20
Pl. 0
Pl. 1
Pl.2
Pl.3
Pl.4
Pl.5
M1
M2
M3
M4
M5
M6
M7-8
M9-10
M11?
S1
S2
S3
S4
or
S4
0.035
0.025
0.015
SYSTEMS TRACKS
TRANSGRESSIVE
HIGHSTAND
LOWSTAND
MRS (Maximum Regressive Surface)
SB (Sequence Boundary)
FALLING STAGE
UNDETERMINED
MFS (Maximum Flooding Surface)
OTHERS
Offlap break
SLOPE APRON
SLUMPS / DEBRIS FLOW
BASEMENT NATURE
SDR
Seaward Dipping Reflectors
T.C
Transitionnal Crust
Beira High
Continental Crust
SEQUENCES
Third order sequences (Laskar, 2011)
Second order sequences (50 - 3 My)

Figure 10